INSTITUTO TECNOLÓGICO Y DE ESTUDIOS SUPERIORES DE MONTERREY
CAMPUS MONTERREY

SCHOOL OF ENGINEERING
GRADUATE PROGRAMS

DOCTOR OF PHILOSOPHY
IN
INFORMATION TECHNOLOGIES AND COMMUNICATIONS
MAJOR IN MICROSYSTEMS

MEASURING EMERGENT POLLUTANTS WITH ELECTROCHEMICAL REDOX PROCESSES AND DYNAMIC MICROFLOW CONTROL

By

José Manuel Rodríguez Delgado

May 2015

Instituto Tecnológico y de Estudios Superiores de Monterrey
Campus Monterrey

School of Engineering
Graduate Program

The committee members, hereby, certify that have read the dissertation presented by José Manuel Rodríguez Delgado and that it is fully adequate in scope and quality as a partial requirement for the degree of Doctor of Philosophy in Information Technologies and Communications, with a major in Microsystems.

_____
Dr. Graciano Dieck Assad
Tecnológico de Monterrey
Advisor

_____
Dr. Marc J. Madou
University of California, Irvine
External Advisor

_____
Dr. Sergio O. Martinez Chapa
University or Institute Name
Committee Member

_____
Dr. Roberto Parra Saldivar
Tecnológico de Monterrey
Committee Member

_____
Dr. Victor Hugo Perez Gonzalez
Tecnológico de Monterrey
Committee Member

_____
Dr. Cesar Vargas Rosales
Director of Research and Graduate Programs
School of Engineering

Declaration of Authorship

I, hereby, declare that this dissertation titled, Dissertation title and the work presented in it are my own. I confirm that:

- This work was done wholly or mainly while in candidature for a research degree at this University.
- Where any part of this dissertation has previously been submitted for a degree or any other qualification at this University or any other institution, this has been clearly stated.
- Where I have consulted the published work of others, this is always clearly attributed.
- Where I have quoted from the work of others, the source is always given. With the exception of such quotations, this dissertation is entirely my own work.
- I have acknowledged all main sources of help.
- Where the dissertation is based on work done by myself jointly with others, I have made clear exactly what was done by others and what I have contributed myself.

_____

José Manuel Rodríguez Delgado
Monterrey, Nuevo León, México
May 2015

Dedication

Thanks to my father and mother for their unconditional confidence, support, patience, and encouragement. You were my main motivation for pushing through this work.

Acknowledgements

I would like to express my deepest gratitude to my family for their support, my father Jose Manuel Rodriguez Gutierrez, my mother Leticia Marlene Delgado Jaramillo and my sisters Melissa Marlene Rodriguez Delgado and Leslie Ivette Rodriguez Delgado, their support kept me going forward this long road.

Also would like to give my thanks my thesis committee, advisor Dr. Graciando Dieck Assad, for his help in this research work and guidance, Dr. Marc Madou for all the interesting projects and input on this work, Dr. Sergio O. Martinez Chapa, Dr. Roberto Parra Saldivar and Dr. Victor Hugo Perez Gonzalez for all their support during these years.

Special thanks to my friends at Tecnológico de Monterrey and University of California, Irvine and thanks to Tecnológico de Monterrey for their support on tuition and CONACyT with the support for living

MEASURING EMERGENT POLLUTANTS WITH ELECTROCHEMICAL REDOX PROCESSES AND DYNAMIC MICROFLOW CONTROL

by

JOSÉ MANUEL RODRÍGUEZ DELGADO

Abstract

The expansion of urban areas and their increase in population has led to a gradual deteriorate of natural sources, especially water resources with the increase of emergent pollutants finding their way to these. Emergent pollutants are chemicals used on daily basis previously unregulated but start to affect the environment when bigger concentrations start to accumulate form human waste and industrial processes. This research work proposes two research methodologies for the detection and control of emergent pollutants in water, first one is an impedance measurement of the sample and second one is an electrochemical measurement.

The impedance measurement uses an interdigitated capacitive sensor in a resistance-capacitance circuit for the detection change in impedance of a sample under analysis. Comparing to a control sample impedance, the system can detect changes in impedance, indicating a difference in the dielectrical properties on the sample under test. Results indicate a clear difference between samples with different dielectric properties but a lack of identification of the compound responsible of this change. The second proposed measuring system, electrochemical measurements, helps to identify these molecules. The electrochemical test is based on the cyclic voltammetry technique in which an oxidation or reduction reaction is induced by a change in voltage on the sample. The change in voltage and measurement of currents is done with three electrodes submerged in the sample a working electrode that measure the current generated, a counter electrode for potential sweep and reference electrode to maintain the voltages constant with respect to a known chemical reaction. Measurement of the current peaks from this methodology allows a clear identification of compounds and their concentrations, solving the problem of identification of compounds from the impedance technique.

Table of Contents

List of figures

List of Tables

Chapter 1: Introduction

Water Pollution is increasingly studied and research has conducted into new methodologies for new pollutant detection having sensors and control systems to diminish threshold levels, aiming for minimization of health hazards. Tests and experiments involving electrochemical techniques have produced high resolution results in detection of emergent contaminants in urban municipal water reservoirs using hardware and software systems under non ideal conditions [1]. The most common techniques to determine the presence of emergent contaminant in water has been off-line techniques that verifies the element contents in specialized laboratories and corrective actions are taken after some lead time from the water works utility companies around the world [2]. Optic technique detection systems have also been used by fluorescent detection that requires several specific conditions and specifications to obtain accurate results [3], [4]. Bio-impedance analysis allows the detection of permittivity dielectric changes of a capacitive sensor system and using impedance spectrometry, the concentration of pollutants have found. The interdigitated capacitive sensors have the ability of increasing the surface interaction with the formed dielectric in such a way that huge changes in impedances can be detected, in liquid water sensing, if a proper bridge system is used in the instrumentation hardware [5]. Moreover, using bio-impedance electrodes by electrochemical reactions is possible to detect REDOX reactions that will create current gains in capacitive electrodes that could provide enough sensitivity to detect pollutant thresholds for on-line determination of emergent contamination in liquid water. This research proposes the use of several electrochemical techniques to design a complete detection and verification system for water pollutant detection in reservoir systems.

This research presents the development of a methodology towards detection and measuring of different kind of emergent pollutants in water such as phenols and anti-bacterials. The methodology uses Bio-impedance and REDOX amplification techniques to

design a prototype for water liquid detection system based upon capacitive transducers. This chapter discusses:

1. Research motivation
2. State of the Art
3. Problem Statement
4. Objectives
5. Main contributions
6. Thesis Organization

1.1 Justification

The development of techniques for detection, controlling and monitoring hazardous water contaminants is a serious concern that intends to provide procedures to prevent health risks in populations and communities. A new problem in the area of water contaminants is the rise of emergent pollutants, which are substances previously not regulated and now are emerging due to the human activities so far. Research performed on their effects on living organisms classifies those pollutants as dangerous for the natural environment and living beings in the whole ecosystem [6], [7]. Some of those new pollutants are generated from human consumption products and general human activities. Products such as industrial additives, personal care solutions, pharmaceutical creams, analgesics, cleaning products, medicines, and steroids, are among these emergent contaminants and constitute a heavy load to eliminate from the life cycle.

The control and tracking of those contaminant substances is extremely important during their whole life cycle, because they could degrade to even more toxic and harmful sub-products than the original compound. New regulations and standards for new sensor devices have not been completely developed and more analytic, dynamic and efficient detection methodologies are required to control the pollutant levels in municipal water

reservoir systems. In 1994, the World Health Organization (WHO) classified phenol compounds as a hazardous water contaminant when released to the environment [8]. United States Environmental Protection Agency (EPA) in their guideline EPA-HQ-OW-2008-0553 recommends for phenol criteria for human health of less than 10,000μg/L and 300μg/L for organoleptic effects (eg. taste, odor). In Mexico, Comision Nacional del Agua (CONAGUA) the norm NOM-127-SSA1-1994 indicates a limit to phenol in potable water below 1μg/L. Expensive equipment and techniques for phenol detection make hard to implement cost effective and user friendly monitoring systems [9] and most of the time those pollutants make their way to nature before any detection is done, generating harmful risks to the ecosystem. A great opportunity exists to develop technologies for early detection of phenols and other harmful pollutants, using less expensive techniques and portable equipment. This work proposes a solution to this problem by developing custom and pollutant specific technology based upon electrochemical measurements and using novel carbon-MEMS electrodes produced by photolithography and miniaturization techniques.

1.1.1 State of the art

Electrode structures at low frequencies with small dimensions relative to the wavelength of the stimulation signals can be modeled as an interconnection of lumped passive or active electrical components. When the signal are either RF or beyond (>1MHz) this model consists of a two port network and its analysis can be found in many microwave engineering books [10]. The precise characterization and modeling of electrode structures are important in the continuous monitoring of different electrochemical processes such as phenolic contaminants reacting with laccase enzyme where reactance variations are detected by electrical circuits. Also, microfluidic biosensors and electrodes have been successfully tested in experimental set ups with promising applications such as: the development of a micro-flow injection amperometric biosensor system to determine the glucose content of

pharmaceutical injections [11]; dielectric spectroscopy and dielectrophoresis to sense changes in dielectric properties of cells [12]; different dielectric techniques used to measure cell viability and their utility [13]; characterization of dielectric properties of oil palm biocomposites [14]; and analyses of the frequency domain characteristics of a single-cell covered microelectrode impedance for cellular biosensing applications [15].

In addition, impedance spectrometry has been used to determine dielectric characteristics of biological substances. Impedance spectrometry has provided remarkable developments with the following important contributions: impedance characterization of cell-electrode interface using an equivalent circuit approach [16]; development of capacitive impedance spectroscopy (CIS) to investigate the electric properties of electrochemical materials [17]; cell manipulation and analysis using dielectrophoresis and micro-electrical impedance spectroscopy in chromaffin and red blood cells [18]; measurement of impedance in biofluids to examine the impact of the length and concentration of free-floating double-stranded DNA molecules [19]; and the use of a resonant sensing electrode structure having an external inductor to sense human blood cells [20]. RF and MW signal stimulation have been used in bioprocessing to characterize dielectric properties of materials such as: moisture content in grains and in considering dielectric heating applications of agricultural products [21] ; evaluation of the RF safety of mobile phones in terms of specific absorption rate [22]; development of a microwave nondestructive evaluation to measure dielectric properties of liquids [23]; measurement of the scattering transmission parameters to determine the dielectric properties of wheat, corn and soybeans [24]; and measurement of dielectric properties of homogeneous isotropic medium using microwave frequency signal stimulation [25].

Current methodologies for detection of pollutants use mass spectrometry in combination with High Performance Liquid Chromatography (HPLC), Gas Chromatography [9], [26] or Raman Spectroscopy [27], [28]. Figure 1.1 illustrates one of this instruments, a HPLC machine for detection of trace pollutants in water.

Those methods use samples taken from an already polluted water reservoir and comparison of the concentration results to a reference sample. The concentration difference between measured and reference samples generate a differential value of concentration which is used to estimate the pollutant content. Results from these methodologies are very accurate and detect concentrations in the order of parts per billion (ppb) [29]. However, their use is limited due to the following drawbacks:

a). Time to run (lead time).

b). Time to move a sample form the source to the laboratory.

c). Pre-concentration of samples. Need a sample preparation with specific concentrations before the test is made.

d). Lack of continuous monitoring reduces the usefulness of this technique for measurements in situ.

Figure 1.1: High Performance Liquid Chromatography (HPLC) instrument

New methodologies involving electrochemical measurements combined with new transducer materials are changing the concept of portable laboratories. Instrumentation can be developed to monitor small arrays with appropriate transducers, which measure target contaminants and they are miniaturized to form the so called lab-on-a-chip devices [30]. Those new instruments use sample size in the order of microliters to study the content values to provide a complete concentration analysis. An example of transducers having those characteristics are tiny carbon micro-electrodes built by micro-fabrication techniques such as photolithography. Figure 1.2 shows an interdigitated carbon microelectrode which is used as a water liquid capacitive transducer to sense pollutant concentration in liquid water [31]–[33].

This research focuses on carbon capacitive electrodes to develop a low cost, fast lead-time, and suitable for on-line applications. We estimate that this methodology will prevent the mobility and time lag problems presented with the HPLC and Raman technologies.

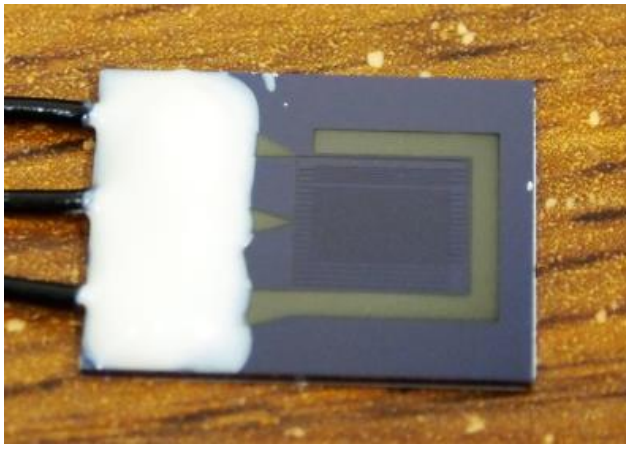

Figure 1.2. Carbon Microelectrode transducer showing interdigitated capacitive sensing scheme

1.2 Problem Statement

Current methodologies for detection and control of pollutants rely on advanced hardware that is found only in specialized laboratories and methodologies that require a time consuming sample processing. Pretreatment of samples is required to obtain a signal related to the quality of a water sample from a natural, industrial or local water source under monitoring. This research proposes a simpler and direct approach to the detection of these pollutants with electrochemical methodologies and state of the art carbon electrodes to achieve similar results.

1.3 Project Objectives

The goals of this research are:

- To analyze the characteristics of a selected group of emerging pollutants.
- To develop transducer prototypes, using carbon microelectrodes fabricated by photolithographic processes, for measuring physical characteristics of liquid water samples.
- To design a system for determination of electrochemical characteristics in liquid water samples having a selected group of emergent contaminants such as phenols.
- To test new techniques for REDOX amplification, applied to phenol and anti-bacterial detection in water, coming from carbon microlectrode transducer prototypes in controlled electrochemical process.
- To test CD-microfluidics methods to implement liquid water pollutant sensors in capacitive transducers embedded into the CD.
- To develop the required graphical programming software in LabVIEW to for measuring and controlling a selected group of emergent pollutants in liquid water reservoirs.
- To perform a statistical validation analysis to determine the resolution and threshold characteristics of the prototype´s transducer technology, comparing those to the pollutant concentration norms dictated by national or international health organizations.

1.4 Main Contributions

The main contribution of this research is the development of a full blown methodology to design, analyze, characterize and test a transducer that monitor the presence of phenols and specific emergent contaminants in liquid water reservoirs. The transducer prototype is tested for the maximum definition, discrimination and resolution to allow a continuous sampling comparable to the pollutant threshold levels posed by national and

international standards for potable water. Moreover, the system will work on-line, having a fast lead time, with graphics programming that permits quick adaptation to different reservoir environments and to consolidate a low cost solution for municipal water sampling. The sensor device used by the transducer prototype is based upon the principle of capacitive bio-impedance and REDOX electrochemical amplification, through the ionic interchange over a four terminal potentiostat system. Finally, the transducer prototype will be compatible to the CD-microfluidics technology and statistical analysis upon the prototype outcomes is performed to validate the expected features such as resolution, REDOX amplification and capacitive electrode characterization.

1.5 Thesis Organization

This research methodology and dissertation laboratory work is presented in a sequence of seven chapters that contain their own introduction and summary. Chapter 1 describes the introduction, justification, literature search, problem description, objectives, main contribution and thesis organization. Chapter 2 develops a review to the theoretical background related to this research, explaining different techniques and methods that validate the prototype experimentation. The chapter also provides a solid background to the fundamental principles used to physically validate the expected results in the experimental phases of the research. Chapter 3 analyzes the first approach for the detection of emergent pollutants. This first method measures the physical properties of water liquid samples having a capacitive transducer with interdigitated copper electrodes. This elementary sensor prototype is characterized by bio-impedance measurements using a hybrid voltage divider (HVD) and a vector network analyzer (VNA) to validate and verify the consistency of the impedance results at different operating frequencies. Chapter 4 describes the water pollutant detection strategies using electrochemical methods such as of cyclic voltammetry (CV) and square wave voltammetry (SWV), having platinum and carbon as working electrodes.

Chapter 5 illustrates the use of electrochemical reactions for the detection of emerging pollutants using C-MEMS (carbon micro electro mechanical systems) microelectrode technology. The C-MEMS electrodes are fabricated using photolithography processes and they consolidate an interdigitated capacitive sensor capable to perform REDOX inter-finger reactions to enhance the electrochemical gain. Improved and more sensitive measurements are obtained, compared with traditional electrochemical methods that use larger electrodes, using a new potentiostatic circuit that detects the working and active currents of the device. Chapter 6 introduces the design and test of a rotating platform for the analysis of liquid water samples inside a CD-microfluidic device that uses centrifugal forces to move water through different chambers inside the disk. This platform will be compatible to implement liquid water capacitive transducers where processes such as heating and cooling are combined with chemical reactions and movement, to improve and accelerate the on-line water sampling results from experimentation. Finally, Chapter 7 concludes the dissertation focusing with the discussion of the figure of merit of the prototype design, the methodology and the future application of this on-line procedures aiming a closed loop implementation to enhance the pollutant-removal and stability of water reservoirs for communities.

Chapter 2: Theoretical Background

To fundament the work done on this document, this chapter covers concepts that are of interest and used during several experiments and includes basic concepts and information of emerging pollutants, methodologies and technologies and how these interact for the development of a physical platform for detection of contaminants.

2.1 Emergent Pollutants

The increase on the number of products that reach our daily lives from manufacturing and pharmaceutical industry increased the amount of emissions produced from the industry and human consumption of those products. Most of these emissions have sub products that are not regulated and recent research shows that they are dangerous for the environment. Some of these contaminants are illustrated in table 2.1 which outlines some of the compounds used and the related molecules derived from these [6], [34].

Table 2.1 Compounds and related examples of emergent pollutants

Compounds	Examples
Pharmaceuticals	• Acetaminophen • Diclofenac • Diazepam • Ibuprofen
Flame retardants	• Tetrabromo bisphenol A • Diphenyl ethers
Antimicrobials	• Triclosan
Steroids and Hormones	• Diethylstilbestol • Estradiol

	• Estriol
Surfactants	• Alkylphenol

From table 2.1, a substance that is commonly used in a chemical or physical process is considered an emergent pollutant when is found outside the environment in which is used. From these pollutants, some of the more studied are presented next, describing their characteristics, uses, and risk if found outside their main applications.

Bisphenol A (BPA)

This molecule is one of the most produced chemicals in the world, is used in several products as an essential component of polycarbonate, commonly in the form of plastic containers like water bottles, toys, tubing, epoxy resins for beverages and food cans.

Even through it is required for a fabrication wide variety of products, current research indicates that exposure to bisphenol A can influence the development of health problems in humans and animals. Bisphenol A is known to be an endocrine disruptor which can mimic estrogen and is related to problems in the development of the reproductive and metabolic systems. It is also linked to an increased incidence of problems in the cardiovascular system, as well as in organs like the liver, kidney and pancreas [35]–[41].

Hydroquinone (HQ)

Belonging to the phenol family, the uses for this compound includes the manufacturing of dyes, photographic developers, manufacturing of rubber, pesticides, cosmetics and depigmenting agents in dermatologic preparations. Another use for hydroquinone is therapy for hyperpigmentary disorders with topical hydroquinone [42].

Even though hydroquinone has many applications, toxicological research reveals an increase in renal adenomas in male F344 rats and cell leukemia in female F344 rats [43], [44] , and cause kidney damage and acute myeloid leukemia in the human body [45]–[49].

Nonylphenol (NP)

Belonging to the phenol family, nonylphenol is used a surfactant for cleaning and industrial processes, fungicides, pesticides, detergents. Nonylphenol also acts as an endocrine disruptor and causes harmful effects on the human body inhibiting endogenous hormone actions and causing cancer [50]–[52]. Due to the risk involved for humans, studies of the kinetics and pathways of nonylphenol [53]–[55] are important to reduce the emission of this chemical to the environment.

Triclosan (TCS)

Used as an anti-micro biocide in toothpaste and soaps, this molecule is added to cleaning products to kill bacteria in the human body (soaps) and mouth (toothpaste). It is also added to cosmetics, polymers and textile fibers for anti-bacterial consumer products.

When triclosan reach wastewaters and soil, it is absorbed by aquatic life and plants, increasing the accumulation of triclosan, affecting fertilization, development of embryos [56], growing of algae and increase of bacteria resistance to triclosan [57], [58].

Ibuprofen (IBU)

Ibuprofen is a propanoic acid (a small, natural occurring acid with a carboxylic group [C(O)OH]) with analgesic, antipyretic, anti-inflammatory properties for treatment of inflammatory and painful diseases. It is excreted by humans under treatment because is not fully metabolized, reaching the sewers and concentrating in wastewater.

The aquatic ecosystem is affected by this drug, as it inhibits growth, causes lysomal membrane destabilization and disrupt antioxidant and detoxifying enzyme activities [59]–[62].

Diclofenac (DCF)

Non-steroidal anti-inflamatory drug used for treatment of rheumatoid disorders with similar characteristics to ibuprofen. Is not absorbed completely in the human body and excreted to sewers and wastewater.

High concentrations of diclofenac in bodies have a negative effect on them, presenting histopathological effects, liver lesions, kidney lesions, gastrointestinal lesions, cardiovascular lesions, sub-cellular effects, genotoxicity and estrogenic effects [63]–[69]

Metformin

Is a biguanide antihyperglicemic agent, used worldwide for treatment of type-2 diabetes mellitus that has the advantage of lowering serum glucose levels [70]. Even though metformin is not linked to emergent pollutants, detection is important for dosages control in diabetes patients and minimize the risk of cancer related to it [71]–[76]

Glipizide

Is used as a sulfonylurea hypoglycemic agent for treatment of non-insulin dependent diabetes mellitus. As with metformin, control of glipizide doses is desired in diabetes patients for minimization of negative effects [77]–[80].

Dopamine

This hormone and neurotransmitter is not considered an emergent pollutant and is hard for it to go to water resources where it can cause harm to aquatic life. Is involved in various functions in the brain like reward learning, exploration, preparation and execution in goal directed behavior. Deficiencies in the neurons that regulate this hormone are related to neural disorders like Parkinson disease, bipolar disorder and schizophrenia [81]–[84].

This work for detection of emergent pollutants use electrochemical techniques that can be applied to detection of dopamine increasing the scientific application of the current detection system.

2.2 Detection Schemes

The rising problem of emergent pollutants requires the implementation of monitoring and detection systems to control the rate of emissions to the environment. Some of these schemes are based on the measurement of electrical and chemical characteristics of the pollutants to identify the principal pattern that differentiates one molecule form another. For the identification of these products, bioimpedance and electrochemical techniques are used in this research to characterize these compounds.

2.2.1 Bioimpedance

Impedance is a physical characteristic of matter to oppose an electrical current generated by a differential of potential applied to it, commonly in the form of a voltage. The focus on bioimpedance is how the physical characteristics of a biological sample resist the flow of current between a pair of electrodes. Depending of these physical properties, the material may behave in a different way to the voltage applied to it, allowing or resisting the flow of current in the material. A common setup to measure impedance is referenced in figure 2.1. The use of two electrodes of area "A" placed parallel between the sample to measure and apply a direct current (DC) or alternate current (AC) voltage "V" and measure the electric current "I" in the circuit. The relation between voltage and current is known as Ohm law (equation 2.1) and represent how the impedance (R in DC and Z in AC) and is a characteristic of the biological sample measured interact with the voltage and current.

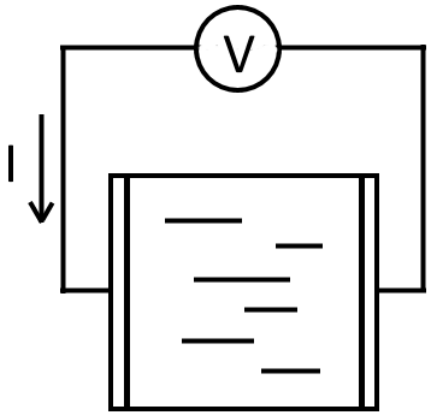

Figure 2.1.Diagram for measurement of impedance of a sample

$$I = \frac{V}{R} \tag{2.1}$$

When using an AC voltage, attention to the impedance of the sensor itself must be subtracted from the results, due to the capacitive effect of the parallel plates adding to the impedance effect. This also can be used to characterize the sensor as shown in chapter 3.

2.2.1 Electrochemical Schemes

Electrochemical measurements are another technique for the characterization of reactions and physical properties. These measurements objective is to find the way a specific set of chemicals in an reaction interact with each other through the electron exchange between analytes and ions by the carefully research and control of chemical reactions using differences in concentrations and potentials between electrodes. Our interest is the study of the electric currents generated by the transport of charge between theses chemical reactions for the characterization of the species under observation.

Generally, the reactions we want on electrochemical measurements are between the electrodes of interest and the electrolyte in contact with them, forming an electrochemical cell in which the reaction occurs in the interfaces between electrodes and electrolyte as shown in figure 2.2.

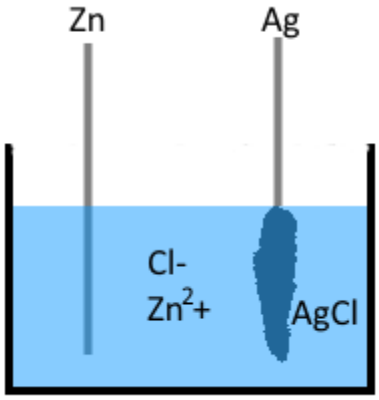

Figure 2.2. Typical electrochemical cell with electrodes of Zn and Ag wire covered with AgCl immersed in a $ZnCl_2$ solution

A potential between electrodes of an electrochemical cell is generally present, indicating the differences in electric potential between the phases in the cell. This potential affects the flow of energy between interfaces. The measurement and control of this voltage allows a change in the in the direction and rate of charge transfer in the cell.

Inside the electrochemical cell two independent half reactions occur, each one at the two electrodes which respond different to the interfacial potential difference in each electrode. Normally only one reaction is of interest in these systems, the electrode in which this reaction happens is named working electrode (WE). The second electrode is then standardized with a known reaction, this second electrode is the reference electrode (RE). Since the reference electrode has a fixed potential, changing the potential between electrodes changes the potential of the working electrode with respect to the reference electrode. Controlling the potential on the working electrode to a high negative value increases the energy of the electrons on the working electrode enough to transfer electrons from the

working electrode to the electrolyte, this is a reduction current. This effect can also be reversed, lowering the electron energy on the working electrode with positive voltage creates an oxidation current from the electrolyte to the working electrode these potentials are called standard potential (E^0) and they are related to the chemicals in the system. When measuring the potential between the working and reference electrode with a current passing through them, a small voltage drop is included in this measurement and equal to iR_s where R_s is the resistance of the solution between the electrodes. To minimize this effect, a third electrode called Auxiliar or Counter electrode (AE or CE) is used in the electrochemical cell. With this three electrode scheme, iRs is mostly removed from the measurements.

2.3 Microfabrication Schemes for Carbon Sensors

Development of sensors at micron sizes (1×10^{-6} meters) requires the use of micro manufacturing techniques commonly used on MEMS (Micro Electro Mechanical Systems) technologies. For Carbon MEMS (C-MEMS) the process starts with a clean silicon wafer with or without an oxide layer on the surface depending of the desired characteristics or etching procedure. This wafer is then coated on a thin layer of photoresist, which is an organic polymer sensitive to ultraviolet radiation and placed in a resist spinner (figure 2.3) to distribute evenly and to the desired thickness photoresist over the wafer depending of the centrifugal force program.

After coating a wafer with photoresist, a process of soft baking is introduced to improve adhesion and remove stress from the photoresist by heating the wafer according to the desired characteristics. The next process is to engrave a pattern on the photoresist with help of a UV light and a mask (figure 2.4) with a desired pattern printed over it and placed between the UV light and wafer. This technique is known as photolithography and engraves the pattern of the mask depending of type of photoresist. For a negative photoresist, UV light reacts in the exposed zones of the wafer rendering insoluble to solvents those parts, creating

a negative print of the mask on the wafer. In positive photoresist the mask protects from UV light the photoresist, duplicating the pattern from the mask.

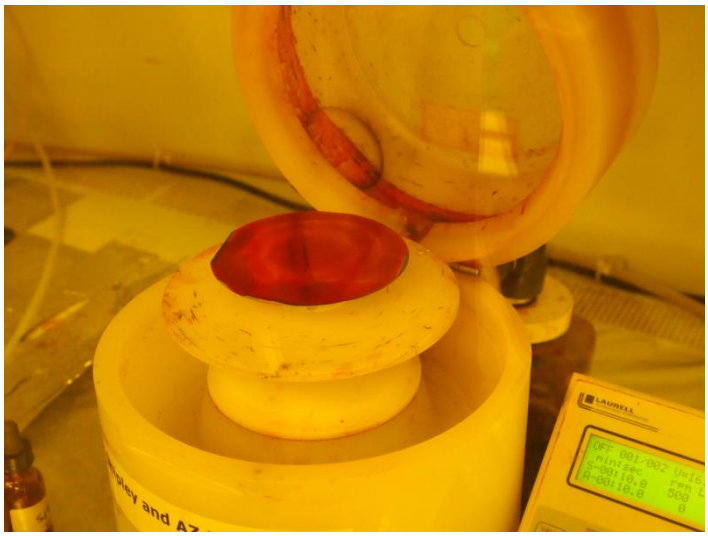

Figure 2.3: Resist Spinner with wafer covered in photoresist

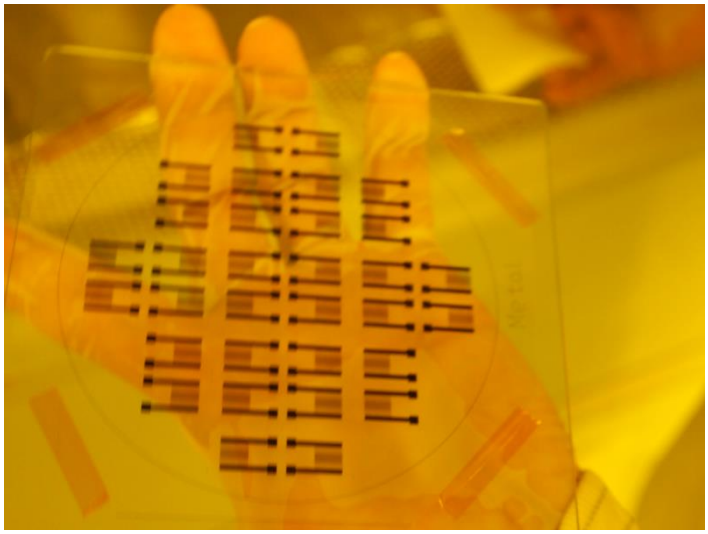

Figure 2.4: Mask for photolithography on positive photoresist

After stripping unwanted photoresist from the wafer using solvents, the pattern etched on photoresist can go to pyrolysis. In this step, the wafer is put inside a furnace at a very high

temperature in a nitrogen environment; this is to induce carbonization of the pattern without burning it out with oxygen. At the end, carbon microelectrodes are obtained and ready for test (figure 2.5).

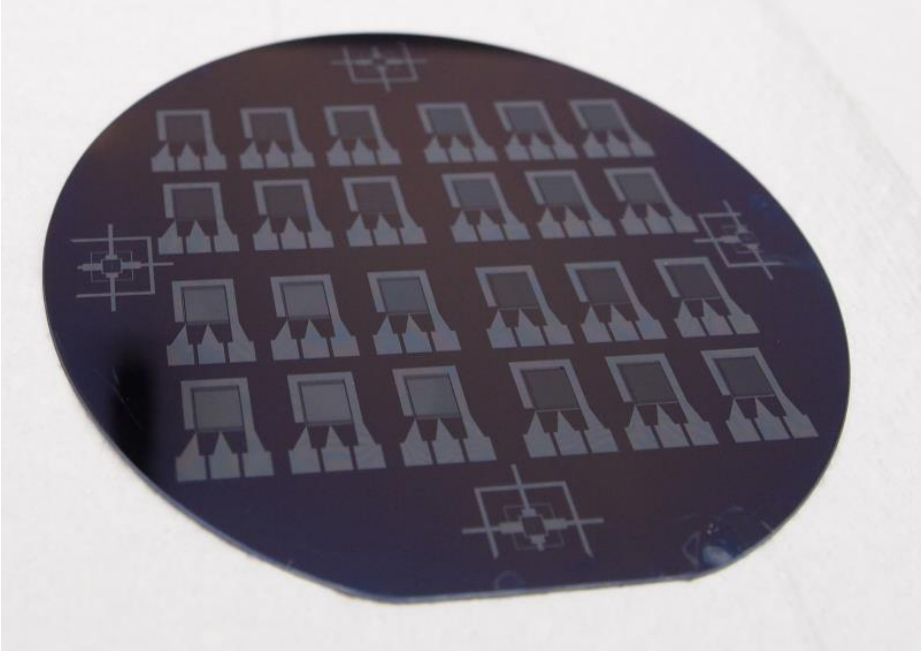

Figure 2.5: Finished Carbon Electrodes over Si Wafer

2.4 Data Processing

At the moment to analyze results from experiments, most of the time, the raw data must be processed to obtain significant information form signals that most of the time contains noise from external sources and artifacts. Data analysis is required to extract useful information from raw data and present results of statistical importance in a clear way for an easy analysis. Several techniques are implemented in this research to improve the raw data and present graphs in a clear way for a better understanding in the phenomena taking place.

2.4.1 Anova

Analysis of Variance (Anova) is a statistical technique for comparison between groups. Provides a statistical hypothesis test of whether or not the means of several groups are equal. Useful in comparing (testing) three or more means (groups or variables) for statistical significance. The statistical test is performed calculating the variance between samples called mean square between samples (MSB) and variance within samples or mean square within samples (MSW) and estimating the variance of populations, σ^2 [85].

With the values of MSB and MSW we can calculate a test statistic F as:

$$F = \frac{Variance\ between\ samples}{Variance\ within\ samples} = \frac{MSB}{MSW}$$

That is related to the F distribution with parameters $k - 1$ and $n - k$, where k is the number of groups and n the number of data values in samples. With the F distribution a p-value is returned, which indicates under the null hypothesis that all samples in X are drawn from groups with the same mean. If p is near zero, it casts doubt on the null hypothesis and suggests that at least one sample mean is significantly different than the other sample means. Common significance levels are 0.05 or 0.01.

2.4.2 Digital Filters

Removing noise from signals is an important task for analysis and processing of information within the raw data measured. Without a clear signal, critical information may be lost and phenomena in the experiment remain hidden. Digital filters are the proposed solution for processing of noisy signals and improvement of the information.

Digital filters process the information form the signal and amplify or reduce the desired characteristics of interest. Depending on how the digital filters respond to an impulse

function, they are classified in two categories, Finite Impulse Response (FRI) and Infinite Impulse Response (IIR). The difference in FRI and IIR filters is that FRI filters output is based only in coefficients and their interaction with the input signal, while IIR filters output depends form the input and previous results from the output as a reclusive system response. For this work FRI filters are implemented with two algorithms, Zero-Phase filter and Savitzky-Golay filter.

Zero-Phase filter is a type of filter that process the signal from the first element of the data to the last one, and then reverse the data and run a new analysis thought the filter. The output of this filter returns a signal without a zero phase distortion as the name indicates.

Savitzky-Golay filter are also called smoothing polynomial filter or least squares smoothing filters are implemented in noisy signals with a large frequency span. The advantage of this filter is that they not remove important information from high frequencies mixed with noise but at a disadvantage of not minimizing noise at the same level of other FRI filters.

2.5 Summary

An increasing necessity for detection, identification and control of emergent pollutants due to the increase of industrial human activities and waste produced by human activities. Several of these emergent pollutants were not classified as contaminants until just some years ago. This change came after several test and observations on common chemicals revealed how they impact negatively life on affected environments and present a hazard to organism in close contact to these pollutants.

For detection of these contaminants, two methodologies are proposed, impedance detection and electrochemical detection. Impedance method relays on the physical characteristics of the sample to oppose an electrical current called impedance, due to an electrical potential between two or more electrodes. A limiting factor in the impedance

methodology is the measurement itself which reveals a change of impedance but not the cause of this change indicates a process is modifying the physical characteristics of a sample with respect to a control sample but we cannot determinate what the direct reason is. The second method, electrochemical detection, use chemical reactions for detection and identification of compounds dissolved on a sample. Detection and identification in this method occurs by doing a reduction and oxidation reaction between interfaces of electrodes and solution by a change in potential on the electrodes of the system and a measurement of the generated currents. Plotting voltage versus current, the current graph reveal the characteristics of the solution and identification of peaks and slopes relate the results with associated chemicals.

Depending of the type of detection, different kind of electrodes are needed. For impedance detection, electrodes can be of simple materials like copper or aluminum and can use basic geometries of parallel plates to complex geometries like interdigitated electrodes to toroid electrode systems. For electrochemical detection, material that facilitates the chemical reactions are needed, like carbon or platinum and the geometry of these is more important for the chemical reaction kinetics leading to geometries that reach micrometer dimensions.

Measurements obtained from these methodologies also need some kind of validation, one way is the use of statistic methods like ANOVA that compares results between them and give a clear relation of how likely are related results and experiments. Before a comparison is important to remove noise from the data first with digital filters to make sure comparisons and validation is close to ideal results.

Chapter 3: Impedance Techniques

A first approach for detection of pollutants in water is the measurement of the conductivity/impedance in water samples to determine the magnitude that these contaminants change this value. The sensor for these experiments is an interdigitated capacitor made in a printed circuit board (PCB).

3.1 Introduction

A first approach to tackle is the design and electrical characterization of a capacitive interdigitated electrode sensor made on a printed circuit board (PCB) for its use as a proof of concept on detection of phenolic pollutants in water resources. The characterization employed used a Vector Network Analyzer (VNA) to determine the S-parameter model and a Hybrid Voltage Divider circuit (HVD) to determine the low frequency impedance model.

The characterization was performed under two conditions: free air and distilled water as dielectric media. The electrical characterization of the electrodes is performed by means of a VNA in the frequency range 500 KHz to 5 MHz. The measured S-parameters are used to model the electrodes as T or PI equivalent lumped electrical circuit. On the HVD signals up to 500 KHz were used with an oscilloscope having a constant R, measurements on voltage and phase were carried out on the capacitive sensor, C, to obtain the reactance parameters.

A test with the HVD and the electrode was performed using laccase enzyme (benzenediol: oxygen oxidoreductase; EC 1.10.3.2), as biorecognition element to bring specificity to the assay. The enzyme was immerse in a distilled water and media composed by a mixture of phosphate buffer and ABTS (3-ethylbenzothiazoline-6-sulfonic acid) to emulate the effect of polluted water with phenolic compounds. The present work characterizes the design of interdigitated electrode capacitive sensors to perform measurements of pollutants in water using two methods. The laccase from Pycnoporus sanguineus, an enzyme with wide substrate specificity for the phenolic substrates [86], [87] was incorporated to the electrode array to be used as biorecognition element. The

characterization methodology compares the performance of the sensor prototype using both, a VNA and an HVD, to detect capacitive changes at specific frequencies. The aim of the study is to probe the use of a simple and inexpensive circuit such as the HVD to detect pollutants in contaminated water

3.2 Detection

The specifications for characterization and potential application of interdigitated capacitive sensor structure considered in this study are: operating frequencies of 500 KHz, 2.0 MHz and 5.0 MHz, and copper electrode printed on a standard PCB. This prototype characterization and testing are based upon two methods:

1. The interdigitated capacitive sensor structure forms a transmission media having scattering parameters (S type) which can be transformed to impedance parameters (Z type). The final results provide a T-type impedance or Π-type model developed from the reciprocal network characteristics as explained in the methodology section. The measurements were performed using a VNA (Rhodes & Schwarz ZVB-8, BW up to 2 GHz) considering three transmitting media: air, water and biological material.
2. The interdigitated capacitive sensor structure forms the reactive part of a hybrid voltage divider (HVD) network which has been calibrated using a 3.3 KΩ resistor to provide a capacitance range from 60 to 1000 pF when air, water or contaminated material is used as a dielectric material in field experiments.

For the characterization and evaluation of the electrical parameters in the interdigitated electrodes forming the capacitive sensor, two methodologies were used at frequencies of 500 KHz, 2 MHz and 5 MHz using a VNA and using a simple voltage divider circuit operating at 500 KHz. Figures 3.1 and 3.2 show schematic diagrams of both methodologies: VNA and HVD.

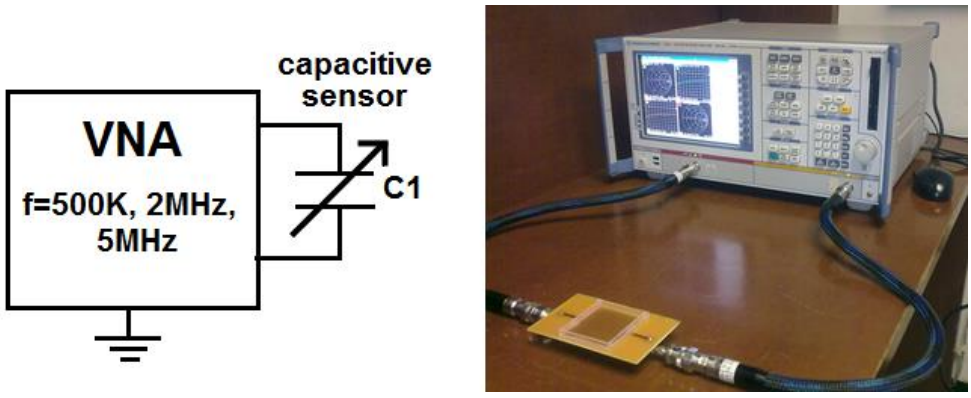

Figure 3.1: Schematic diagram (Left) and picture of the VNA connections to the capacitive sensor for testing (right).

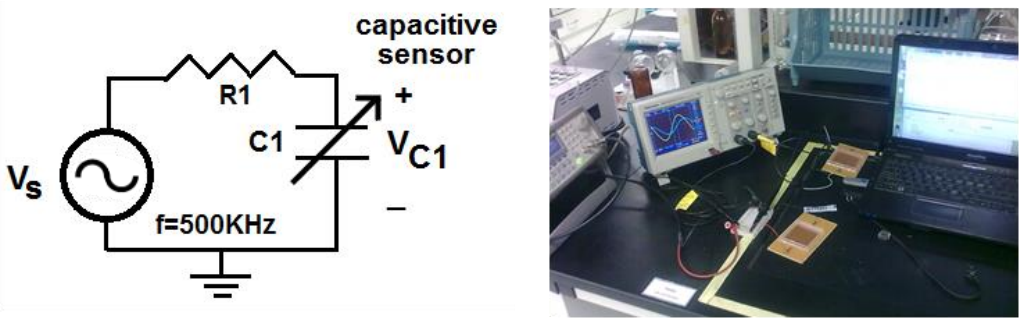

Figure 3.2: Schematic diagram (Left) and picture of the Hybrid Voltage Divider connections to the capacitive sensor for testing (Right).

The use of these two detection schemes provides useful information to predict the behavior of the physical phenomenon taking place on the capacitive sensor.

3.2.1 Capacitive Sensor using VNA

In the VNA equivalent voltages, currents, and their related impedance/admittance matrices become an artificial abstraction tool for characterization and modeling of the capacitive sensor. A capacitive sensor structure where high-frequency stimulation is performed to describe the behavior of biological media can be modeled as a two port network

(Figure 3.3a). A good representation of this appropriate network for direct measurements having incident, reflected and transmitted waves can be obtained by the so called scattering matrix or S-matrix. The scattering matrix provided a complete description of the two port network and their parameters can be calculated using network analysis techniques. Moreover, those scattering parameters can be also measured by the VNA and then converted to impedance form. The scattering matrix [S] was defined in terms of incident and reflected voltage signals as follows:

$$\begin{bmatrix} V_1^- \\ V_2^- \end{bmatrix} = \begin{bmatrix} S_{11} & S_{12} \\ S_{21} & S_{22} \end{bmatrix} \begin{bmatrix} V_1^+ \\ V_2^+ \end{bmatrix} \tag{3.1}$$

$$[V^-] = [S][V^+] \tag{3.2}$$

Where Vi^- represented the amplitude of the voltage wave reflected from port i, Vi^+ represents the amplitude of the voltage wave incident to port i, and the specific elements of the S-Matrix were defined as follows:

$$S_{ij} = \left. \frac{V_i^-}{V_j^+} \right|_{V_i^+ = 0 \; for k \neq j} \tag{3.3}$$

Which means that S_{ij} is determined by driving port j using incident signal wave Vj^+ and measuring the reflected wave amplitude Vi^- at output of port i. Thus, S_{ii} describes the reflection S-parameter seen looking into port i when the other port is terminated in matching load (usually 50 Ω) and S_{ij} describes the reflection S-parameter from port j to port i when the other port was terminated in matching load (usually 50 Ω). A transformation of the S-Matrix model was convenient to illustrate an impedance model as shown in the figure 3.3a. The impedance model was expressed from the transformation from currents to voltages as follows:

$$\begin{bmatrix} V_1 \\ V_2 \end{bmatrix} = \begin{bmatrix} Z_{11} & Z_{12} \\ Z_{21} & Z_{22} \end{bmatrix} \begin{bmatrix} I_1 \\ I_2 \end{bmatrix} \tag{3.4}$$

Where Z_{11} is the input impedance, defined as the ratio of voltage V_1 to current I_1 measured at port 1 with open output port 2 or I_2=0 (forward measurement), Z_{21} is the forward transfer impedance, defined as the ratio of voltage V_2 to current I_1 measured with open output port 2 or I_2=0 (forward measurement), Z_{12} is the reverse transfer impedance, defined as the ratio of voltage V_1 to current I_2 measured with open input port 1 or I_1=0 (reverse measurement), and Z_{22} is the output impedance, defined as the ratio of voltage V_2 to current I_2 measured at port 2 with open input port 1 or I_1=0 (reverse measurement). To transform the scattering matrix or parameters S to impedance matrix Z, the following equations are used:

$$Z_{11} = Z_o \frac{(1+S_{11})(1-S_{22})+S_{12}S_{21}}{(1-S_{11})(1-S_{22})-S_{12}S_{21}} \tag{3.5}$$

$$Z_{12} = Z_o \frac{2S_{12}}{(1-S_{11})(1-S_{22})-S_{12}S_{21}} \tag{3.6}$$

$$Z_{21} = Z_o \frac{2S_{21}}{(1-S_{11})(1-S_{22})-S_{12}S_{21}} \tag{3.7}$$

$$Z_{22} = Z_o \frac{(1-S_{11})(1+S_{22})+S_{12}S_{21}}{(1-S_{11})(1-S_{22})-S_{12}S_{21}} \tag{3.8}$$

Where Z_o is the matched characteristic impedance which the electrode structure has been calibrated, in this case this is exactly 50 Ω and it is symmetrical seen from port 1 or seen from port 2. The capacitive sensor shows mirror impedance matching looking from port 1 and looking from port 2. Therefore, an equivalent electrical impedance representation shows the T topology which is illustrated in the figure 3b. In this case, the transformation to the impedances Z1, Z2 and Z3 for the T model was given as follows:

$$Z1 = Z_{11} - Z_{12} \tag{3.9}$$

$$Z2 = Z_{22} - Z_{12} \tag{3.10}$$

$$Z3 = Z_{12} = Z_{21} \tag{3.11}$$

Likewise a reciprocal model, the Π-equivalent admittance can be obtained from the impedance parameters as follows:

$$Y_{in} = Y_{11} + Y_{12} = 1/Z_{11} + 1/Z_{12} \tag{3.12}$$

$$Y_{out} = Y_{22} + Y_{12} = 1/Z_{22} + 1/Z_{12} \tag{3.13}$$

$$Y_{12} = Y_{21} = 1/Z_{12} \tag{3.14}$$

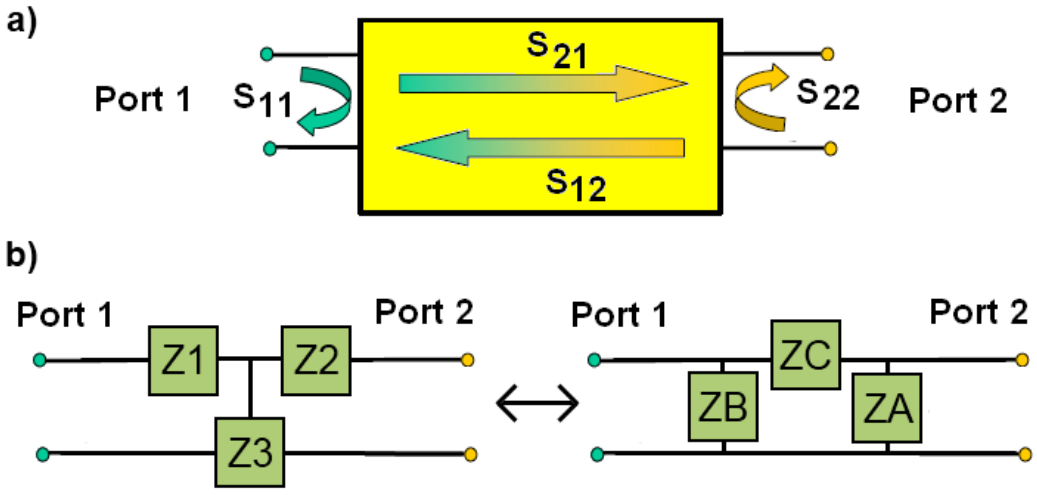

Figure 3.3: a) Representation of a two port network with parameters [S] to describe the behavior of the network. b) Visualization of the two port network as a T-Π circuit.

T model presents several important characteristics for the capacitive sensor:

1. Z1 increases the sensor´s equivalent impedance at Port 1 if Port 2 is open circuited.
2. Z2 increases the sensor´s equivalent impedance at Port 2 if Port 1 is open circuited.
3. Z3 represents the shunt impedance usually connected to the ground plane of the sensor system and typically is described by an RC network with specific permittivity and resistance depending upon the biological media.

Summarizing the methodology we described the following procedure to obtain the impedance parameters of the electrode structure.

1. Connect the Interdigitated electrodes capacitive sensor to the SMA (Sub-Miniature version A) coaxial RF (Radio Frequency) cables, 1 for each side of the electrodes.
2. Connect SMA cables to the vector network analyzer.
3. Configure the vector network analyzer to read and measure the S parameters.
4. Use S parameters to calculate Z parameters using equations 3.5 to 3.8.
5. Use Z parameters to calculate T-Π circuits using equations 3.9 to 3.14.

3.2.2 Capacitive sensor using HVD

The HVD (hybrid voltage divider) consisted of an RC network where the capacitive sensor was connected to ground and it was adjusted at the half power point. This is, at the operating frequency of 500 KHz, the resistance value equals to the sensor´s capacitive reactance such that the detection and measurement of the impedance were performed roughly at the point where the impedance magnitude equals the value of R (a standard 3.3K carbon resistance having a tolerance of 5%). The figure 3.2 shows the typical hybrid voltage divider. Parasitic effects and cable resistances were neglected in this experiment.

The magnitude and phase of the capacitive sensor´s output voltage, V_{C1}, are given by:

$$|V_{C1}| = \frac{1}{\sqrt{1+(\omega_o R \times C1)^2}}|V_S| \tag{3.15}$$

$$\angle(V_{C1}) = -\arctan[\omega_o R \times C1] \tag{3.16}$$

The HVD detection showed some important characteristics:

1. The device behaved as a low pass filter of the input signal V_S with a phase going from 0 to -90°.

2. According to this behavior, the magnitude of the output voltage reduced to 70% of the DC value when $\omega_o=1/RC$.
3. When the capacitive reactance $X_C=1/(\omega_o C)$ equals the resistance of the divider, R, the magnitude of the output voltage also reduced to 70% of the input signal magnitude (half power point).

Summarizing the HVD methodology we described the following procedure to measure the interdigitated capacitance electrode characteristics as follow.

1. Connect resistor in a series circuit with the capacitive sensor (C1) using interdigitated electrodes. The impedance of the resistor must be close to the impedance (X_{C1}) of the capacitive sensor. Figure 2.
2. Connect the series circuit to a function generator with a sine signal and frequency that results in an approximate value (less than 1% error) of X_C.
3. Connect an oscilloscope channel 1 to the function generator and channel 2 to the capacitive sensor´s electrodes.
4. Measure the peak voltage of both channels and their phase difference; with these parameters we can calculate the angle and magnitude of the impedance in the capacitive sensor, allowing a constant measurement of the impedance changes when a different substance is introduced over C1.

3.3 Capacitance Modeling

Using the design software SOLIDWORKS, an interdigitated capacitor was modeled then the geometry exported to simulation software COMSOL Multiphysics and simulated using electrical parameters to obtain the capacitance. The proposed model contains 50 cooper electrodes equally spaced between them with a length, width and height of 50.3mm, 0.508mm and 0.035mm respectively. The electrodes were separated in two groups of 25 and connected through the same node of 50.3mm by 2.54mm, forming an array where each

electrode is equally spaced a distance of 0.508mm with respect to the neighboring electrode and a separation of 1.016mm between electrodes arrays (see Figure 3.4).

After the design, the prototype was fabricated over a printed circuit board (PCB) with FR4 epoxy (ε_r=4.5) as the dielectric and cooper electrodes. For the simulations, we considered 2 capacitances occurring over the prototype, the capacitance of the FR4 and the capacitance of the surface where the biological samples were measured. For the surface capacitance, air and distilled water were used to compare the change in the capacitance value. Results from the simulations are showed in table 3.1. Conductor and dielectric losses are neglected.

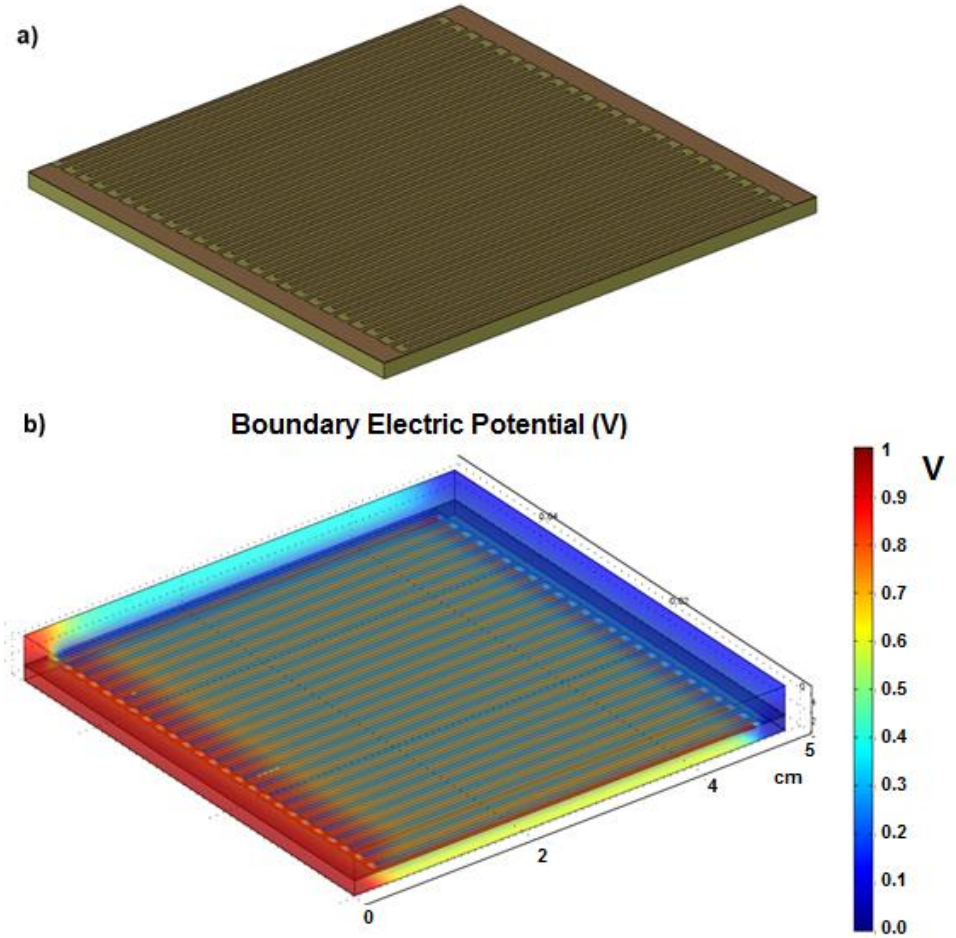

Figure 3.4: Design and simulation of capacitive sensor using interdigitated electrodes. SOLIDWORKS (a) and COMSOL (b) used for design and simulation, respectively.

Table 3.1: Simulation of capacitance values for interdigitated electrodes in COMSOL Multiphysics.

Material	Capacitance	Impedance at 500 KHz
FR4 (εr=4.5)	53.09 pF	-j5.996 KΩ
Air (εr=1)	11.38 pF	-j27.971 KΩ
Distilled Water (εr=80)	905.5 pF	-j0.352 KΩ
FR4 + Distilled Water	958.59 pF	-j0.332 KΩ

These results show that the total capacitance in air for the prototype was 64.42 pF, while the same capacitor with distilled water over the surface was 958.59 pF. Table 1 shows also the impedance calculation at 500 KHz because that is the operating frequency of the sensor with the HVD.

3.4 Testing the Capacitive Model

Fabrication of the prototype was performed using standard PCB and a 50Ω track and SMA connector was added for connection to the VNA. Results obtained from the VNA are in the form of Z-parameters that we used to convert them to a T-Π circuit as showed in figure 3.3b. Results from the VNA are presented in table 3.2 with the equivalent impedances for the T-Π circuit at 500 KHz.

Table 3.2: Comparison between parameters Z and T-Π impedances with capacitive sensor having interdigitated electrodes with air and distilled water

Parameters	Air	Distilled Water
Z_{11}	3.647e+003 -8.967e+003j	1.608e+003 -6.301e+003j
Z_{12}	2.319e+003 -3.539e+003j	1.555e+003 -5.973e+003j
Z_{21}	2.345e+003 -3.497e+003j	1.589e+003 -5.927e+003j
Z_{22}	2.206e+003 -5.084e+003j	1.603e+003 -5.993e+003j
Z1	1.378e+003 -5.388e+003j	5.557e+001 -3.257e+002j
Z2	-1.398e+002 -1.587e+003j	13.847 -66.688j
Z3	2.345e+003 -3.497e+003j	1.589e+003 -5.927e+003j
ZA	2.507e+003 -6.252e+003j	1.974e+003 -7.203e+003j
ZB	1.550e+004 -1.769e+004j	8.322e+003 -3.526e+004j
ZC	3.645e+002 -8.889e+003j	6.982e+001 -3.960e+002j

If we use the Π circuit, we can relate the impedance ZC to the sensor capacitance. Calculating the capacitance from the imaginary part of ZC, we obtained results for distilled water of 803.71 pF and for air is 35.809 pF. These results were also reflected in the measurements of S_{11} and S_{22} parameters which indicate the impedance viewed from the ports 1 and 2 (figure 3.5). Table 3.3 illustrates the real and imaginary parts of parameters S_{11} and S_{22} as a function of frequency for both dielectric media, air and distilled water. The results from air are erratic mostly in the real part. However, results for distilled water, when comparing real and imaginary parts of S_{11} and S_{22}, show errors from 0.26 to 5.19% which is very reasonable for the capacitive sensor prototype.

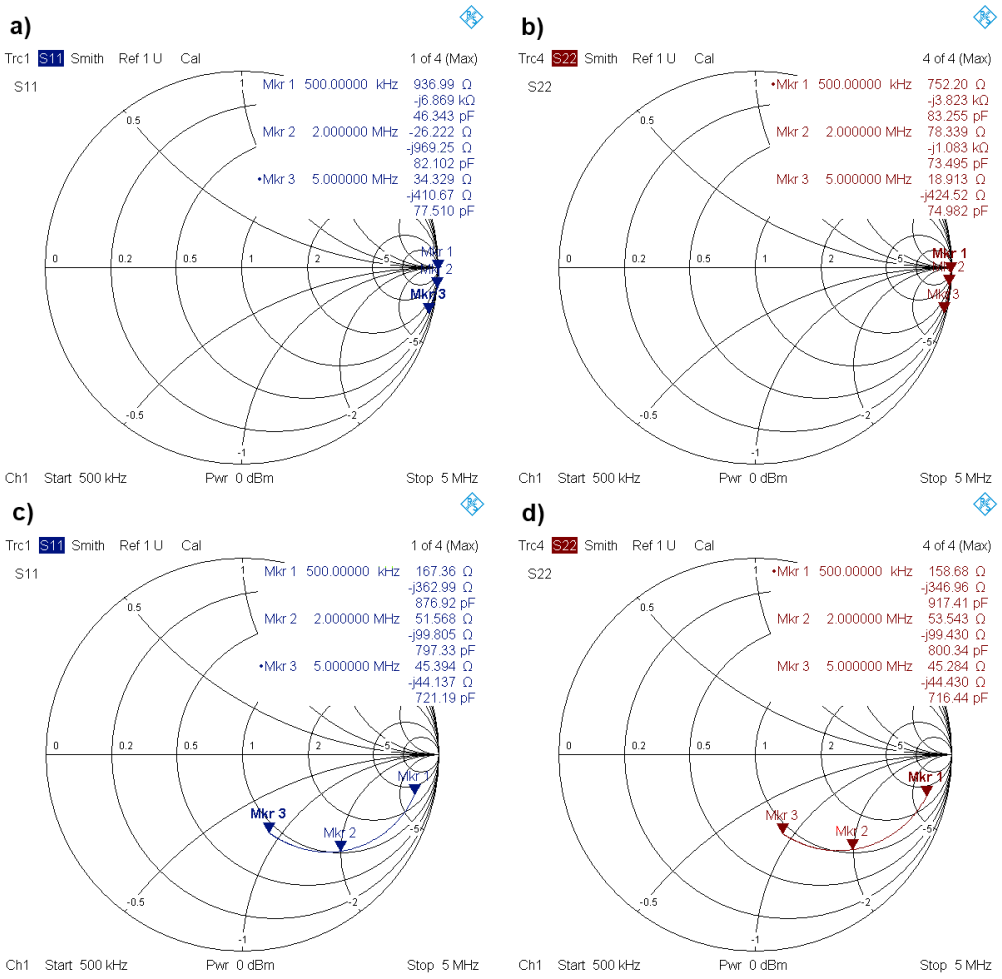

Figure 3.5: Smith Chart plots of parameters S from vector network analyzer. a)S_{11} in air, b) S_{22} in air, c) S_{11} in bi-distilled water, d)S_{22} in bi-distilled water.

Table 3.3: Parameters S_{11} and S_{22} from VNA measurements at different frequencies and consolidated errors for distilled water

Dielectric media	**Real S_{11} Ω**	**Imaginary S_{11} Ω**	**Real S_{22} Ω**	**Imaginary S_{22} Ω**	**Frequency f**
Air	937	-6.87 K	752.2	-3.823 K	500 KHz
Air	-26.22	-969.25	78.34	-1.083 K	2 MHz
Air	34.33	-410.67	18.913	-424.52	5 MHz
Distilled water	167.36	-363	158.68	-346.96	500 KHz
Distilled water	51.57	-99.8	53.54	-99.43	2 MHz
Distilled water	45.4	-44.14	45.28	-44.43	5 MHz

TITLE Table 3.4

Dielectric media	**%Error |Re(S11)Re(S22)|/|Re(S11)|**	**%Error |Im(S11)-Im(S22)|/|Im(S11)|**	**Frequency**
Distilled water	5.19	4.42	500 KHz
Distilled water	3.82	0.37	2 MHz
Distilled water	0.26	0.66	5 MHz

The methodology for the HVD followed the test of the components of the circuit; from the probes of the oscilloscope to the complete circuit is showed in figure 3.2. Calibration

of a function generator to a sine wave of 500 kHz and amplitude of 5 Volts p-p to compare with results from the VNA.

A first measurement was done over the oscilloscope probes to see the capacitance contribution from them into the measurement of capacitance from the electrodes. After the measurement of the oscilloscope probes, the electrodes were connected to the circuit and new measurements were done with air and distilled water. The results obtained from these measurements are presented in table 3.4. If we remove the capacitance of the oscilloscope probes, the measured the capacitance of the sensor in air is 58 pF and in distilled water is 840 pF. Table 3.5 shows a comparison between the sensor capacitance results from VNA and HVD. Errors from 4.21% to 8.43% are obtained with distilled water which allows us to consider the HVD as a very good candidate to detect impedance changes in polluted waters.

Table 3.4: Measurements from HVD operating at 500 KHz

Component	**Resistance (ohms)**	**Va (V)**	**Vz (V)**	**Phase (ns)**	**Capacitance (pF)**
Oscilloscope probe	3300	5.0	3.6	210	84.6
Osc. Probe + Electrodes with Air	3300	5.0	2.72	290	142
Osc. Probe + Electrodes with distilled water	3300	4.96	0.52	380	924

Table 3.5: Changes in sensor capacitance with different media and consolidated errors operating at 500 KHz

	VNA S11 (pF)	**VNA S22 (pF)**	**HVD (pF)**
Air	46.34	83.26	58
Distilled water	876.92	917.41	840

	%Error $\lvert C_{S11} - C_{HVD} \rvert / \lvert C_{S11} \rvert$	**%Error $\lvert C_{S22} - C_{HVD} \rvert / \lvert C_{S22} \rvert$**
Air	25.15	30.33
Distilled water	4.21	8.43

3.5 Results and Discussion

Having the capacitive sensor operating in a HVD, a test using 0.5 ml of laccase enzyme (8 U/ml) produced by the fungus *Pycnoporus sanguineus* was diluted on 7 ml of distilled water and the change in capacitance was measured. After that 0.5 ml solution of 2,7-azinobis (3-ethylbenzothia-zolone-6-sulfonic acid) diammonium salt (ABTS) at 5mM was added to the enzyme solution, mixed and incubated at room temperature. The ABTS was used as analyte of interest during the test, due to its phenolic structure, probing the enzymatic reactivity of the laccase and correlate it with the change of impedance. This compound is widely use as substrate and the reaction can be easily followed by the color changing. During the next 10 minutes the oxidation reaction was monitored where the ABTS loss an electron forming the radical $ABTS^{+}$ which is observed in the solution as a change in color from colorless to an intense green as seen on figure 3.6. After 10 minutes, at the end of the redox reaction, the electrodes did not detect any change in capacitance after the initial change in the first minutes of the oxidation reaction.

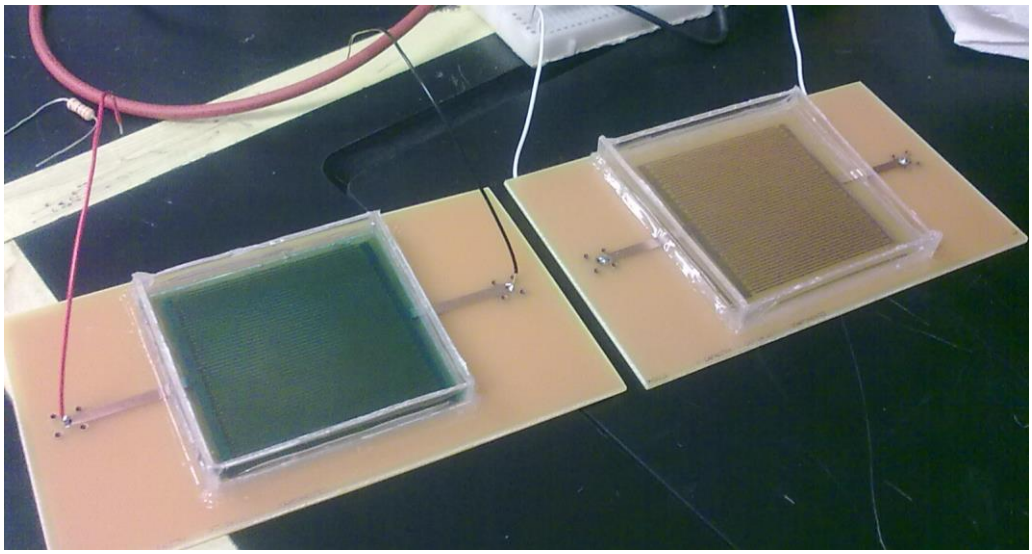

Figure 3.6: HVD capacitive sensors using interdigitated electrodes. On the left is a sample with Laccase plus ABTS at the end of the reaction. To the right is a sample of distilled water.

A second test using 7 ml of phosphorus buffer at 50 mM at pH 7.6 instead of the distilled water was carried out to compare the results from the measurements. The rest of conditions from the previous tests were equated. Results obtained comparing the differences in capacitance during each step of the measurement process with the respective electrical parameters for the electrical setup of the HVD are showed in table 3.6. The table shows changes of 7.9% in calculated capacitance when comparing the phosphorous buffer against the Laccase+ABTS solution. Also, the calculated capacitance from Laccase to Laccase+ABTS on water has a swing from 8.36 nF to 45.5 nF, an increase of 544%, meanwhile on phosphorous buffer the difference in Laccase and Laccasa+ABTS goes from 70.9nF to 177nF, an 249% difference. With the specified parameters from the experiments, we see a clear reduction of the voltage measured on the capacitive sensor due to the frequency of the signal generator and different dielectric properties of the samples.

Table 3.6: Changes in sensor´s capacitance using different samples with frequency of 500 KHz

	Resistance (Ω)	**Va (V)**	**Vz (mV)**	**Phase (ns)**	**Calculated Capacitance (nF)**
Laccase (distilled Water)	3300	4.9	55.58	521.36	8.36
Laccase + ABTS (distilled Water)	3300	4.89	10.01	514.45	45.5
phosphorus buffer	3300	4.89	9.30	508.64	49.1
Laccase (phosphorus buffer)	3300	4.89	6.48	498.41	70.9
Laccase + ABTS (phosphorus buffer)	3300	4.89	2.58	456.76	177

3.6 Summary

Changes in interdigitated capacitive sensors due to physical properties of water samples, phosphate buffer, laccase enzyme, ABTS+ and the reaction between them over the sensor surface were successfully detected using both, HVD or VNA schemes. Differences in the capacitance between simulations in COMSOL and measurement results from VNA and HVD were due to non-ideal conditions in the fabrication of the electrodes and losses not considered on the simulation. Comparison between VNA and HDV measurements of capacitances show errors, of distilled water, of up to 8.43%. Capacitive measurements in the presence of laccase and ABTS indicated that the system was sensitive enough to detect those substances in 7.5 milliliters of solution; from whish 0.5ml corresponds to the laccase enzyme and 0.5 ml to the ABTS+. The response of capacitance between laccase and laccase with ABTS+ results in an increase in capacitance magnitude of 5.44 in distilled water and 2.49 in phosphorous buffer as described in table 3.6.

Comparing the methodologies used between VNA and HVD, results from the VNA are more complex and need interpretation to relate the results obtained from this method to the physical phenomena of a change in dielectric properties of a capacitive sensor. HVD presents results in a simple way with a direct relation between the change in voltages and phases between signals and the increase or decrease of capacitance in the sensor but using more hardware to do those measurements (oscilloscope, Signal Generator) although less complex to use and less expensive than a VNA. HVD also needs an excitation signal with a frequency that allows a measurement of the impedance of the capacitor close to the resistance connected in series.

In table 3.4 an excitation signal of 500KHz is connected to the circuit and the difference in voltages and phase on the capacitive sensor reflects the change of impedance/dielectric permittivity of the sample. Capacity for liquid samples up to 12.5 milliliters can be used over the 5 cm X 5 cm area of the capacitive electrode which is protected from corrosion with a nonconductive epoxy resin with less than 0.5 mm thickness. For bigger liquid samples, the guards around the sensor can be removed and submerged on a bigger sample as a commercial conductivity sensor with the difference that the one designed in this research measures the changes in electric field between the fingers of the sensor instead of a change in different geometries like parallel plates and toroid. The tests performed to measure capacitance changes in the HVD illustrate a valid technique to detect changes in dielectric permittivity with enough sensitivity for simple instrumentation hardware.

Chapter 4: Design and Implementation of Potentiostat Circuit

This section complements the methodology discussed on chapter 3 with electrochemical measurements as a technique that complements the results obtained from an impedance measurement. Electrochemical detection systems can be trained to recognize different kinds of chemical compounds by the characteristics of the reduction-oxidation curves obtained in electrochemical tests. Results from this chapter indicate a clear differentiation between selected contaminants with different concentrations and differentiation between pollutants according to the statistical data and direct measurement of signals form the lab equipment.

Even through these results show a favorable outcome for detection of pollutants, the electrodes used for the measurements, conditions for sample measurement and laboratory equipment required are expensive and are only usable inside the laboratory. With current efforts to develop a more sustainable model for control and detection of pollutants, our aim is to implement a detection system that can provide the same robust results from lab equipment using components and microfabrication techniques that together present an economical solution to this problem at hand.

A first step in this direction was presented on chapter 3 where an impedance sensor developed using only a PCB sensor and a common electrical circuit is enough for detection in capacitive changes in the nanofarad (nF) range. For electrochemical measurements the challenge to measure currents in the nanoampere (nA) range while controlling a variable signal supply using new electrode technology discussed on chapter 2 in a small device represent an opportunity for innovation and a solution with direct applications to the problem of emergent pollutants.

This chapter discusses the design and implementation of a potentiostatic circuit and the results obtained with it using a different array of pollutants and electrodes for comparison.

4.1 Experimental setup with commercial potentiostat

To propose a benchmark on the custom potentiostat, test with commercial hardware was done. Equipment for the electrochemical experiments include the use of a commercial potentiostat 600E form CH instruments, platinum counter electrode, platinum micro working electrode, glassy carbon working electrode and standard Ag/AgCl reference electrode (figure 4.1). The pollutant to measure on this experiment is hydroquinone. Other pollutants were considered for this test but results were not satisfactory, due to absorption problems on the working electrode and non-optimal pH and concentrations. Those other pollutants were glibenclamide, glipizide, irinotecan, metformin and tolazamide. A more extensive review of literature is needed to optimize the parameters for their measurement and is outside the scope of this work and will be researched after the characterization of the custom potentiostat. With the exception of hydroquinone, the other pollutants are used for treatment of diabetes. These samples concentrations are fixed at 100 parts per million (ppm) equivalents to 100µg per 1mL of solution. Their molar concentration is presented also on the figures.

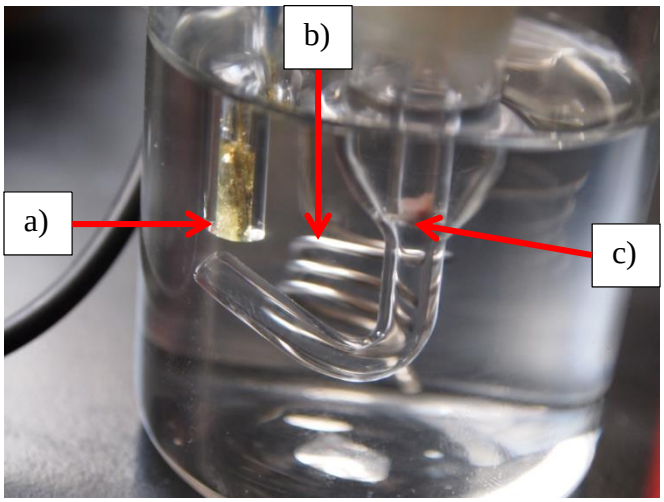

Figure 4.1: Electrodes for electrochemical cell, a) Micro platinum electrode (Working electrode), b) Platinum electrode (Counter electrode), c) Ag/AgCl electrode (reference electrode)

For the detection of these compounds, the principal electrochemical technique used is Cyclic Voltammetry and Square Wave Voltammetry is used for the non-conclusive tests with the antidiabetics. An analysis of the results is also done with ANOVA processing to get the statistical difference between concentrations on a same sample.

4.1.1 Analysis of Hydroquinone and Antidiabetics

The test with hydroquinone presents results for 2 electrodes, first is presented results with the glassy carbon electrode in figure 4.2. Three different concentrations are tested (0.454mM, 0.908mM and 1.362mM) equivalent to 500, 1000 and 1500 µg of hydroquinone. The sample is mixed in a buffer solution of phosphate (PBS) at 0.1mM and pH of 7.2. Scan rate of 50mV/Second is used on the cyclic voltammetry experiment with a triangular wave with range of -0.4V to 0.8V.

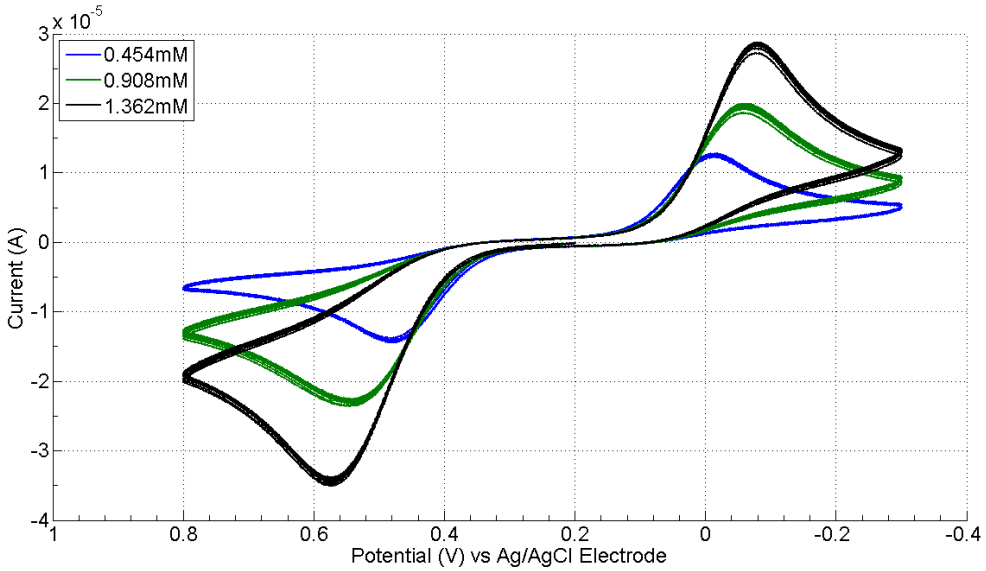

Figure 4.2 Cyclic voltammetry of hydroquinone at 50mV/s on PBS buffet at pH 7.2 with glassy carbon electrode.

Table 4.1 illustrate results of the CV of hydroquinone from figure 4.2, currents at the anodic and cathodic voltages demonstrate an increase in amplitude congruent to the increase of molarity. This result also demonstrates a lineal relation between concentration and current without a big deviation on the excitation voltage versus the voltage of the reference electrode. An anova analysis also demonstrates a statistical difference between different concentrations of hydroquinone in comparison between means. These results are presented in figure 4.3 where clear baps between means indicate a bigger probability of not be confused one concentration between each other.

Table 4.1 Currents and voltages form CV of hydroquinone with glassy carbon electrode.

Cyclic Voltammetry of hydroquinone				
Concentration (mM)	Ic (μA)	Vc (V)	Ia (μA)	Min Va (V)
0.454	12.7×10^{-06}	0.03	-13.7×10^{-06}	0.47
0.908	19.9×10^{-06}	0.06	-23.3×10^{-06}	0.55
1.362	28.7×10^{-06}	0.1	-34.8×10^{-06}	0.58

Another conclusion from the anova test is that an automated system can recognize different concentrations by measuring the means of a test and comparing the results with a calibration curve. This allows for efficient pattern recognition and reliable detection systems for detection of pollutants.

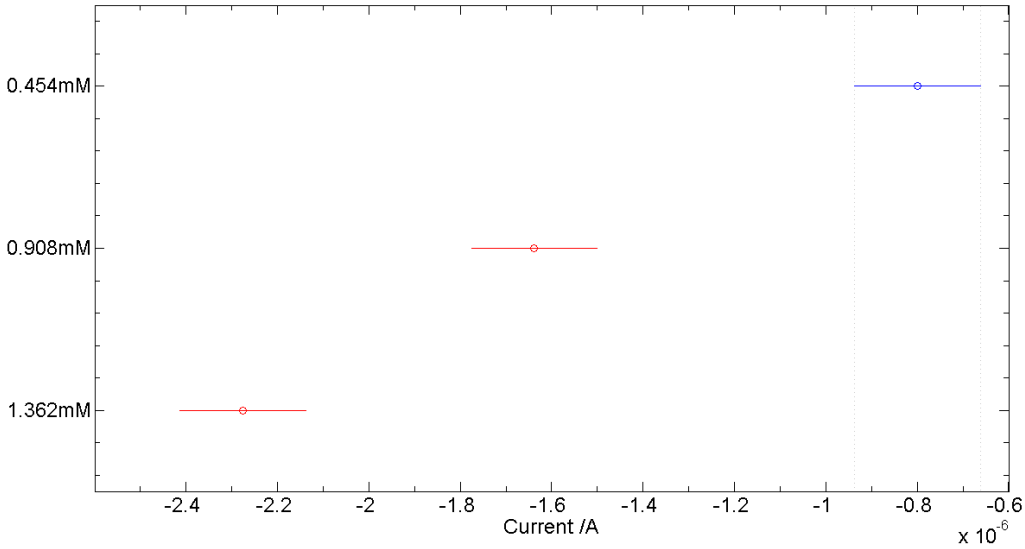

Figure 4.3 Means study form anova test. Results indicate that the means of different hydroquinone test are separated enough for an automated system to recognize them and differentiate concentrations.

Electrochemical test using a platinum micro electrode were less successful on hydroquinone with the same buffer conditions. These electrodes presented absorption problems that decreased their response with the commercial potentiostat, an example on this is presented on figure 4.4.

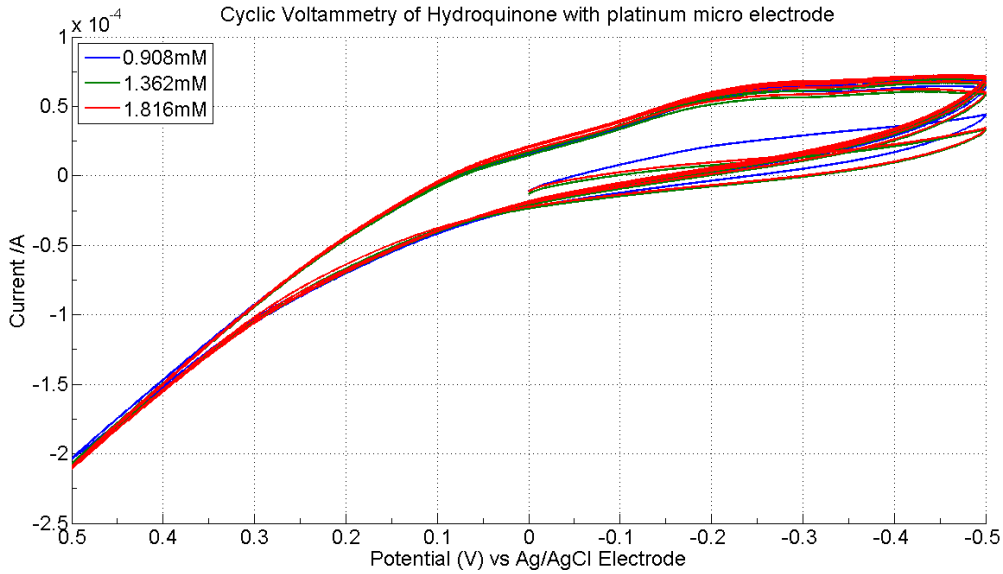

Figure 4.4 CV of hydroquinone with platinum micro electrode. Current graph don't present the characteristics peaks of oxidation and reduction.

The hydroquinone experiment, running with concentrations of 0.908, 1.362 and 1.816mM presented a poor electrochemical result, with an atypical Voltage-Current graph, only a small bump in current at -0.22V is presented but is mostly lost in the measuring process. The anova comparison with platinum also reveals a close mean between experiments, making difficult to have a clear identification of curves based on their concentrations. These results are presented in figure 4.5 and demonstrate that for these experiments, the platinum microelectrode is not an optimal choice for the system.

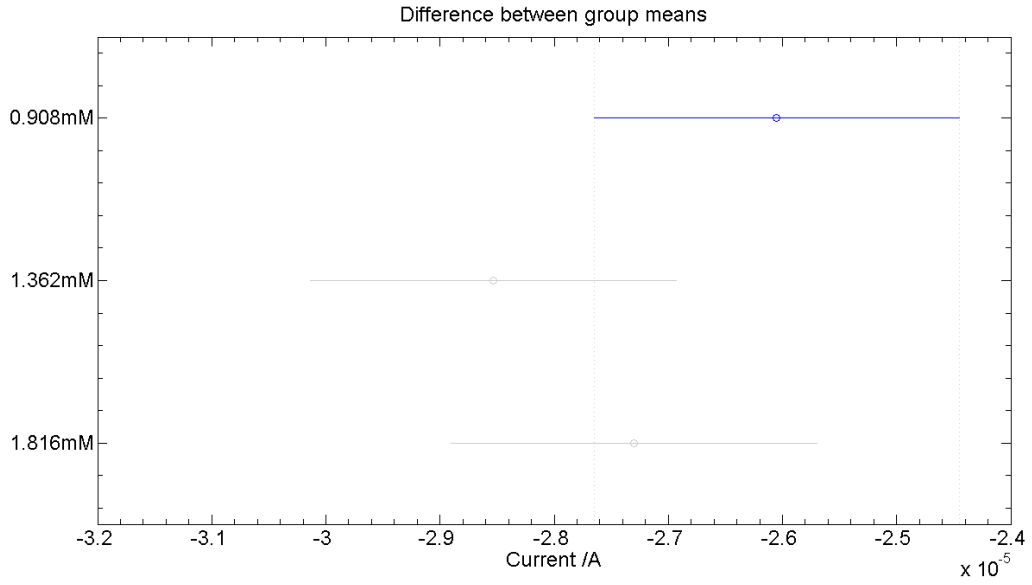

Figure 4.5 Comparison of means between experiments of hydroquinone with platinum microelectrode. Means overlap on each other for all the experiments, making hard to detect which concentration is being run in the experiment.

Other set of experiments with antidiabetics were planned for comparison with hydroquinone, but results from these present atypical current curves that are hard to identify.

An example of these atypical curves is in figure 4.6 where an experiment with glipizide presents only anodic current peaks and decreased amplitude each time the concentration was increased. This strange behavior is mostly caused due to an abortion effect on the platinum microelectrode which decreased the response of it. Also due to the complexity of the molecule, more specific buffer conditions and parameters are needed to get better responses to the applied voltage.

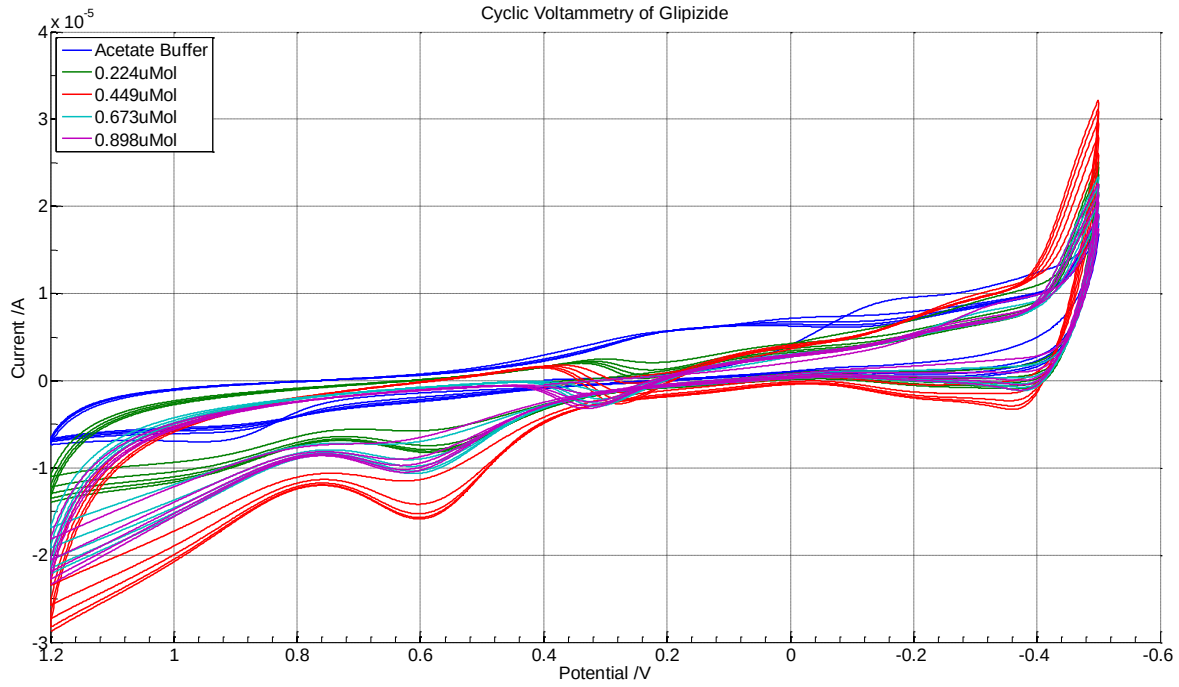

Figure 4.6 Irregular curve of Voltage-Current graph in CV experiment of glipizide due to absorption effect and complexity of molecule.

Due to the problems characterizing the antidiabetics, the test with them will be done after more solid knowledge of their optimal conditions is researched.

4.2 Design of Potentiostatic Circuit

One of the most expensive parts of an electrochemical cell is the potentiostatic circuit that excites and measures the chemical reactions. For laboratory use, professional chemical equipment can do a wide variety of tests and measurements on the electrochemical cell for any different variable that can be measured inside it. The most important one for this research is cyclic voltammetry as seen in section 4.1. The hardware required for a CV measurement must:

1. Control the voltage applied to a counter electrode (CE).
2. Measure the current generated at the working electrode (WE)
3. Keep the potential of the reference electrode (RE) with respect to the counter electrode (CE) at the same potential.

Following these three design rules for the custom circuit, the best component to achieve the best performance is the analog circuit Operational Amplifier (opamp). This circuit can accept positive and negative voltages as their power supply, coinciding with the signals commonly found on CV. It also has a high impedance differential amplifier with a very high gain as input and a low impedance output.

For this custom electronic circuit, the opamp circuit (represented as a triangle commonly in schematics) is present in each step of the circuit in different configurations as is needed depending on how the inputs and outputs are connected. In figure 4.7, the prototype potentiostatic circuit is presented as a collection of different functional blocks, each one with a precise function.

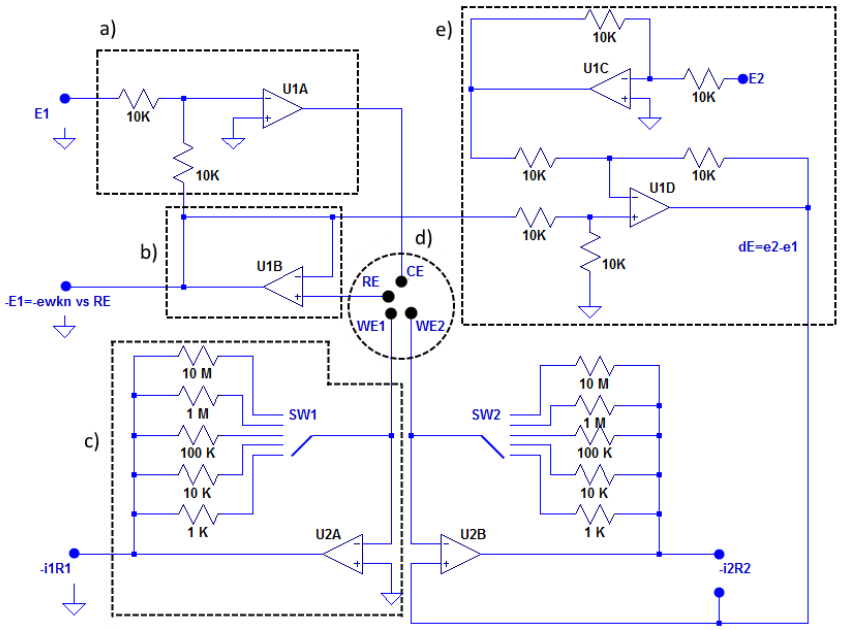

Figure 4.7: Potentiostatic circuit and functional blocks: a) voltage inverter adder, b) voltage follower, c) current follower, d) electrochemical cell, e) voltage subtraction

The first functional block of the schematic (voltage inverter adder) provides the counter electrode with the excitation signal for the CV process. To the excitation signal, the second block (voltage follower) feeds the potential of the reference electrode to maintain a constant reference voltage. The voltage follower maintains the same potential from the reference electrode without changing the electrical currents in it. The working electrode is connected to the current follower. This block converts the current from the working electrode to a voltage equivalent to the current of the system and amplified by the magnitude of the feedback resistors. For this schematic, a second current follower is connected to a second working electrode for current measurements at a different excitation potential. This second potential is obtained from a voltage substractor block that generates a differential signal from the two excitation signals at the beginning of the schematic. This new signal is used as a reference for the current follower of the second working electrode.

4.3 Generation and Measurement of Signals Using LABVIEW and NI myDAQ

With a potentiostatic circuit ready for the electrochemical cell, the excitation signal must be generated and currents from the working electrode measured. The hardware chosen for generation and measurement of signals is the National Instruments (NI) myDAQ. This hardware is a data acquisition system that generates up to two analog signals and measure also two analog signals, enough for a CV application. Generation and acquisition of signals is control by the software Labview, with it, virtual instruments (VI) are implemented for each task in the CV process. The VI implemented contains a signal generator (sine, triangle, random waveform) module which achieves the required characteristics for redox excitation. Another module of the VI is the sampling of the voltage obtained from the potentiostat generated by the current of the working electrode. Finally a digital processing module is included for the filtering and processing of the data acquired from the CV. In figure 4.8, we see the complete system connected to a electrochemical cell, the total footprint of the system is small enough for easy transportation and connection.

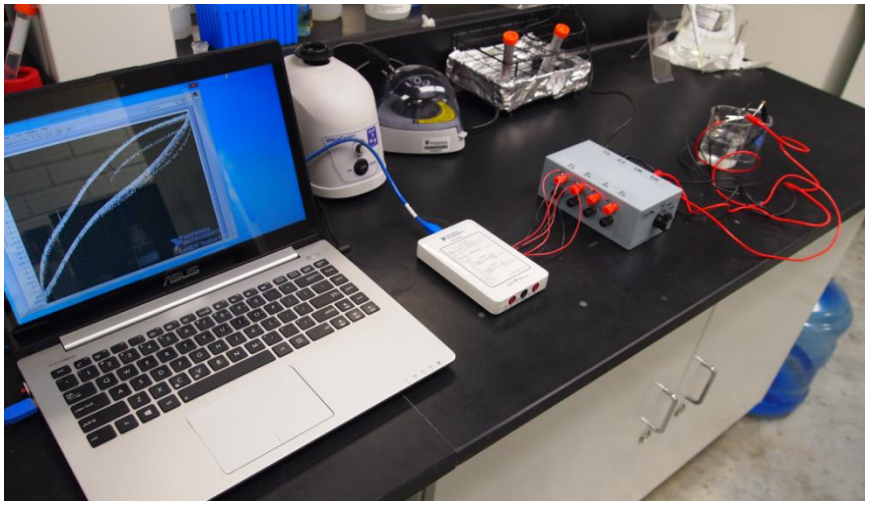

Figure 4.8: Custom electrochemical system. From left to right: 1) Laptop with Labview, 2) myDAQ acquisition system, 3) Potentiostat, 4) Electrochemical Cell

The small footprint and easy connection are two important characteristics for the prototype. This allows an easy transportation and measurements on site, important for a dynamic methodology where the point of interest may be located on difficult terrain or hard to reach places.

4.4 Detection of pollutants with carbon electrodes

With the new potentiostat ready for test, we selected three carbon working electrodes to test with the new circuit (figure 4.9) which register different signals depending of their individual characteristics and areas. The three electrodes are the glassy carbon from previous experiments a flat surface pyrolysed carbon electrode and pyrolysed carbon mat electrode, both made with SU-8 photoresist.

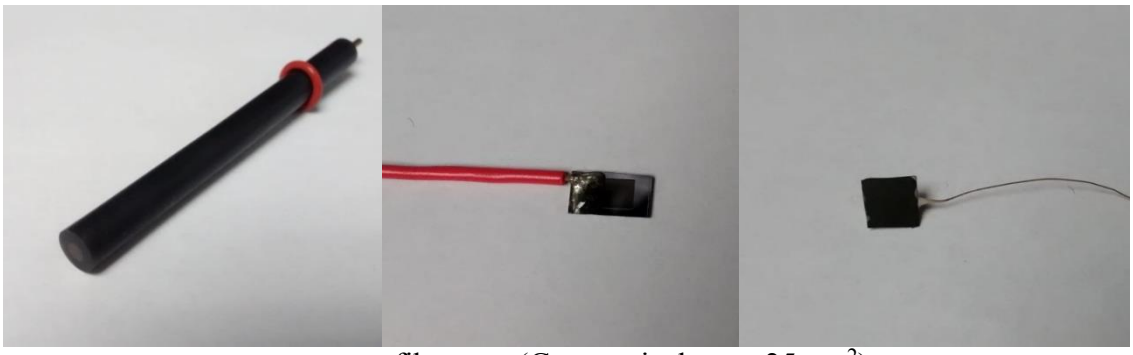

Figure 4.9 Carbon electrodes. From left to right 1) Glassy carbon (Geometrical area: 7mm^2), Flat pyrolysed carbon (Geometrical area: 9mm^2) and pyrolysed carbon fiber mat (Geometrical area: 25mm^2)

The next tests present results with ferricyanide as a test compound and dopamine at different concentrations. Results are presented as current density (A/mm^2) versus voltage to normalize the results due to the difference in areas between electrodes. The first results are presented for ferricyanide with three plots on the same experiment with different working electrode. Conditions for this experiment is:

- Scan rate of 50 mV/s
- Range: -0.2V to 0.6V

- Concentration: 5mMol
- Buffer: Potassium Chlorite (KCl) at 0.5Mol and pH 7.4

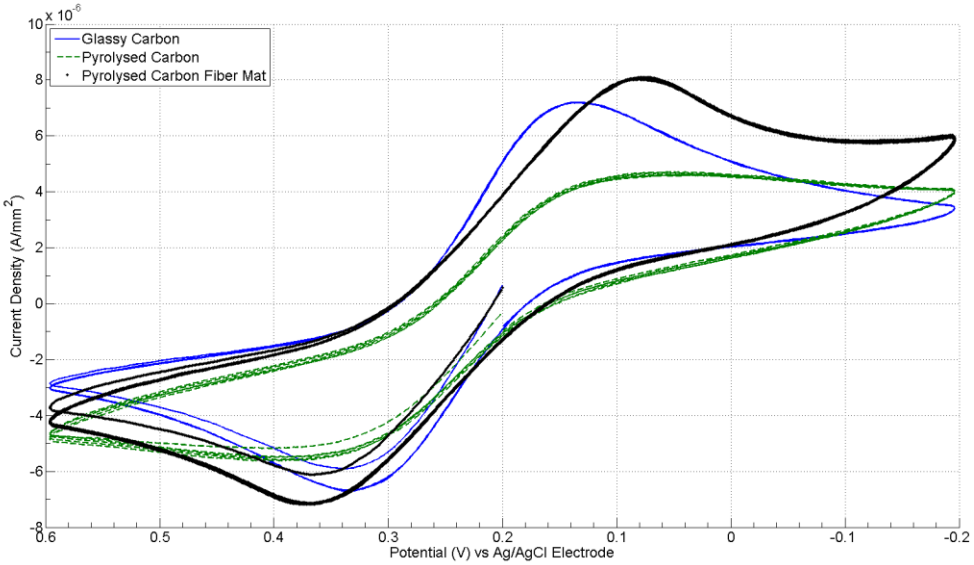

Figure 4.10 Cyclic voltammetry of ferricyanide with three different carbon electrodes using custom potentiostat.

From the current density versus voltage plot on figure 4.10, and data form this same experiment on table 4.2, similar response of carbon mat electrode and classy carbon electrode was measures. A reduced current was present during flat carbon electrode where the current peaks are reduced considerably, even though the shape of the plots are almost the same. The current peaks are bigger at the fiber mat carbon electrode with almost with a difference of around 1µA between this electrode and the glassy carbon one. Current peaks also present almost the same voltages for the current peaks, demonstrating the stability of the process without too much drifting.

Table 4.2 Results for ferricyanide experiment with carbon electrodes with custom potentiostat

Cyclic Voltammetry of Ferricyanide				
Electrode	Ic ($\mu A/mm^2$)	Vc (V)	Ia ($\mu A/ mm^2$)	Min Va (V)
Glassy carbon	$7.19x10^{-06}$	0.14	$-6.68 x10^{-06}$	0.32
Pyrolysed carbon	$4.67 x10^{-06}$	0.06	$-5.59 x10^{-06}$	0.34
Pyrolysed carbon fiber mat	$8.06 x10^{-06}$	0.08	$-7.16 x10^{-06}$	0.37

Next, an experiment with neurotransmisor dopamine, the three carbon electrodes from the last experiment and custom potentiostat, this with the end to see if CV can be obtained with different compounds. The importance of dopamine for brain cells make it an interesting molecule for detection that is not directly related to emergent pollutants, but is affected in the same way than those compounds. Results for this experiment are presented in figure 4.11 for the graph comparison between electrodes and in table 4.3 for the numeric comparison in current peaks. The format is the same as the last experiment with the next parameters:

- Scan rate of 50 mV/s
- Range: -0.1V to 0.5V
- Concentration: 0.02mMol
- Buffer: Phosphate Buffer Solution (PBS) at 0.1Mol and pH 7.4

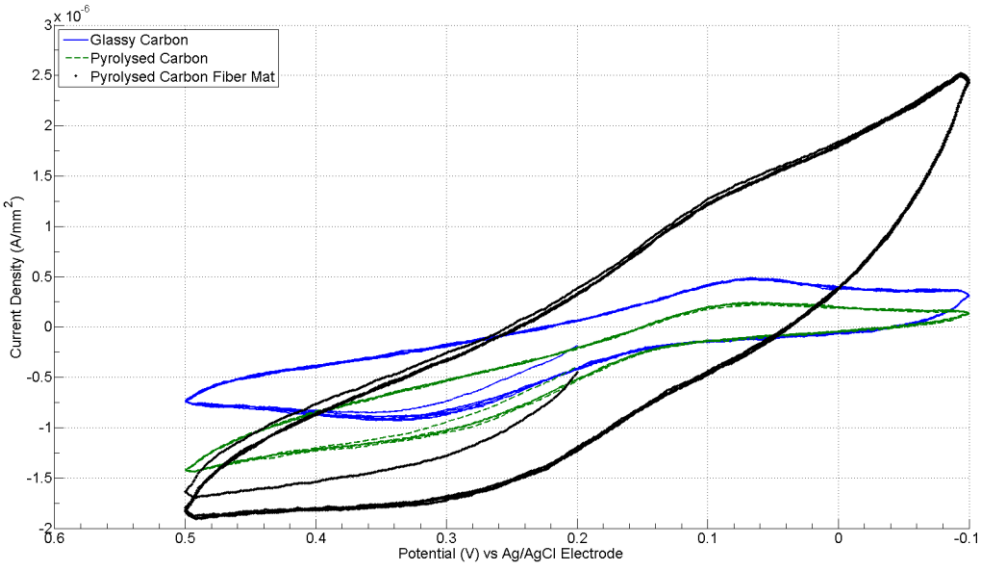

Figure 4.11 Cyclic voltammetry of dopamine with carbon electrode arrays and custom potentiostat

Table 4.3 Peak density currents of dopamine with carbon electrodes and custom potentiostat

Cyclic Voltammetry of Dopamine				
Electrode	Ic (μA/mm^2)	Vc (V)	Ia (μA/ mm^2)	Min Va (V)
Glassy carbon	0.49 x10^{-06}	0.08	-0.92 x10^{-06}	0.32
Pyrolysed carbon	0.23 x10^{-06}	0.08	-1.08 x10^{-06}	0.3
Pyrolysed carbon fiber mat	1.26 x10^{-06}	0.11	-1.7 x10^{-06}	0.3

From the current density plots, the measurement of dopamine has a bigger response with the carbon fiber mat than with the other two electrodes by around three times more on the cathodic peak. Voltages are consistent with the current peaks during the complete scan from -0.1V to 0.5V with clear reproducibility.

A final experiment for the system, an interdigitated carbon electrode with two working electrodes was tested with a ferricyanide solution to see the redox amplification effect on these electrodes. The electrode is based on the one shown on chapter 1 in figure 1.2, to represent the geometry, a microscope image on figure 4.12 shows the structure of this electrode.

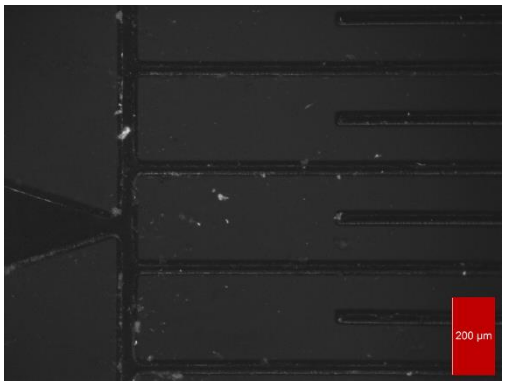

Figure 4.12: Internal configuration of Carbon Interdigitated Electrode Array seen form microscope

Parameters for this test are show below with the added parameter of flow over the electrode to test the effect over redox amplification:

- Scan rate of 50 mV/s
- Range: -0.2V to 0.6V on working electrode one, 0.6V to -0.2V on working electrode 2
- Concentration: 5mMol
- Buffer: Potassium Chlorite (KCl) at 0.5Mol and pH 7.4
- Controlled flow of solution over the electrode of 0 µL/min and 30 µL/min

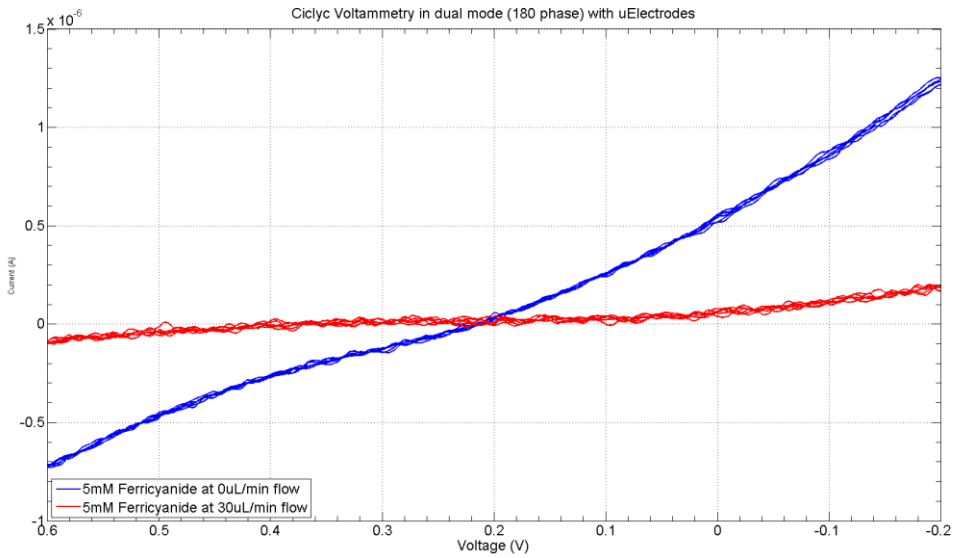

Figure 4.13: Cyclic voltammetry of interdigitated carbon electrodes with ferricyanide solution with and without flow conditions.

As we see from figure 4.13, the response of the current on the interdigitated electrodes is too small with flow of 30 µL/min compared to no flow conditions. This is due to the effect of the flow moving the species being reduced or oxidized from the neighboring electrode to the solution bulk. We also see an increase of current at the voltage peaks that demonstrate an increment of at least 10 of the currents comparing the flow and no flow conditions.

4.5 Summary

This chapter discusses the design of a custom potentiostat that fulfils the needs of a portable electrochemical detector and the test for detection of emergent pollutants. The first test were done with a commercial potentiostat to demonstrate the necessary characteristics of the custom potentiostat and the response of the working electrodes. Electrical circuits that include the operational amplifier circuit are required for their amplification gain and impedance characteristics desirables for electrochemical measurements. Response form this system is controlled by the voltage applied to a voltage inverter added, maintaining the excitation potential with respect to the reference electrode. The current detected by the

working electrode is then introduced to a current follower block which transforms this current to a voltage with an amplification equivalent to the feedback resistor.

To generate and acquire the signals form the potentiostat, a DAQ system is added to the potentiostat, the DAQ selected is the National Instruments myDAQ. This myDAQ provides two analog inputs and two analogs outputs for data acquisition and generation of analog signals for the potentiostat. Labview software is also connected to the myDAQ to generate the excitation signals with the required amplitude, frequency and slope. Data obtained from myDAQ is processed by Labview, filtering and displaying the currents as a function of time or a function of voltage.

A first run with a platinum electrode, commercial potentiostat and hydroquinone demonstrate the current-voltage responses expected for the experiments. Experiments with three different carbon electrodes on a ferricyanide solution as a calibration solution present a similar response, displaying the expected current peaks. A second test with dopamine also illustrates the correct functioning of the device and the differences in current due to the properties of the electrodes. The third test was done with a carbon interdigitated electrode and a ferricyanide solution to demonstrate the redox amplification effect of two working electrodes running the same experiment. With these results the correct operation of the custom potentiostat is proved and reliable information on the electrochemical characteristics of the samples can be obtained from the device.

Chapter 5: Conclusions

This chapter contains a compilation of the research notes and results presented on this document and proposed projects for idea development to further improve these research. At the end of this chapter, two appendixes are presented to expand the information from previous chapters. The first appendix talks about the CD microfluidic platform, a technology that offers a reliable way for sample preparation and measurement that uses centrifugal force for the movement of internal samples on internal sensors. The second appendix illustrates the Labview code used to generate the signals in the cyclic voltammetry and measure the currents from the redox process.

5.1 Conclusions

Detection of emergent pollutants is an important topic of general concern to the urbanized population, due to their increase in use and easy incorporation to water resources. The idea behind this work is to propose a methodology for detection of these pollutants and control the movement of these compounds to minimize their effect to society. Efforts for detection of emergent pollutants were done with electrical techniques for their detection; an example of this is the proposed measurement with electrodes for detection of these compounds with impedance changes.

As discussed in chapter 3, impedance measurement is an economic technique for the measurement of physical properties of a sample under test. The concept is based in a change in the impedance property, resistance to an electrical current, due to a change in the sample. With differential measurements between a control sample and test sample a measurement of impedance can detect if the test sample was changed due to an external compound. Test with water, buffers and laccase demonstrate that impedance chance the moment any of the compounds is added to bi-distilled water. The detection of this change is done with the movement of the voltage vectors in a simple R-C circuit, where the electrodes act as a

capacitor and the sample to measure the dielectric between them. A more complex way to measure this change is to use a vector network analyzer to find the parameters of the capacitor, considering the R-C circuit as a transition line. This impedance property is useful for detection of the change but not for the identification of the compound that was added to cause this change. This detail have big consequences because we cannot know if for example, a water sample is being contaminated with a pollutant or just some common buffer solution. A proposed solution for this problem is the use of electrochemical measurements for the identification of pollutants.

In chapter 4 we start to develop the idea of use electrochemical measurements, in specific, cyclic voltammetry, for the detection of specific compounds in a sample solution. Cyclic voltammetry is a technique based in the principles of oxidation (loss of electrons) and reduction (gain of electrons) due to a potential between electrodes in contact with the sample. Depending of the voltage between electrodes the movement of electrons is due to an oxidation current or a reduction current, these currents increase at specific voltages. Plotting voltage versus current, these reactions present peaks of current at specific voltages, these specific points are precise for the compound being measured, allowing a clear identification of it.

To demonstrate the electrochemical technique, a test with a commercial potentiostat and the hydroquinone compound allows a demonstration of the desired currents in a CV. With the results of this test, we started to design a circuit that can process the same excitation signal for the CV experiment and measure the currents generated. This circuit is based on the operational amplifier circuit, amplifying the excitation voltage in a counter electrode and measuring the current generated on the working electrode. Another characteristic of the circuit is that maintains the potential of the working electrode with respect a reference electrode, without disturbing the potential of this one. Excitation signal and current measurement is done with a National Instruments NyDAQ, controlled by Labview software, also property of National Isntruments.

Testing of the custom potentiostat with ferricyanide and dopamine as custom samples demonstrated the oxidation and reduction peaks of the process. Also the result indicate the difference in current between electrodes is low when the area of the electrode is normalized with the current. A final test demonstrate the effect in interdigitated carbon electrodes and the redox amplification technique, which amplifies the currents due to an increase of the analytes on the surface of the neighboring electrode.

The results on these test where all positive with the exception of tests on a micro platinum electrode, which presented problems with absorption effects, reducing the response of the electrode. Another problem was related with the sample preparation and choosing of parameters for experimentation on anti-diabetics, without a careful experimental setup, results were not representative of the electrochemical characteristics of these compounds.

5.2 Future Research

Test of the custom potentiostat presented positive results, from measuring currents to maintaining excitation voltages, the system worked as expected and obtained congruent data, expected for the chemical reactions. An opportunity to improve this system is presented in the circuit design, current prototypes use a through-hole system for electronic components, more susceptible to noisy signals and contact problems. Changing to surface mount technology can improve the resistance to electrical noise form the power supply and reduce the footprint of the circuit. Another proposed addition is the implementation of a custom analog to digital and digital to analog modules for excitation signals and measurement of currents. These modules can be implemented on the same potentiostat circuit, reducing the dependence of National Instruments hardware, removing the need of an expensive data acquisition system (MyDAQ). A next step in this direction would be the removal of the Labview software, replacing it with a custom made program, improving the speed of

processing and only using the most important functions for generation and measurement of signals.

Further test with new compounds are also needed to verify the expected signals for different kinds of pollutants and find the optimal conditions for those compounds, like the anti-diabetics mentioned before. The system also needs to recognize the differences in current peaks between different pollutants for be a complete detection system. New algorithms are being studied to be implemented for pattern recognition, identification of samples with more than one pollutant mixed on the same sample is desired for future testing.

Lastly, a new sample preparation and measurement platform on CD is being prepared for future experimenting. This CD system can store samples in microfluidic CD's and control the preparation, flow rate, measurement and disposal of the samples inside it. As presented in figure 5.1, the flow chart represents the expected result of complete monitoring system that integrates this CD technology with an improved detection system.

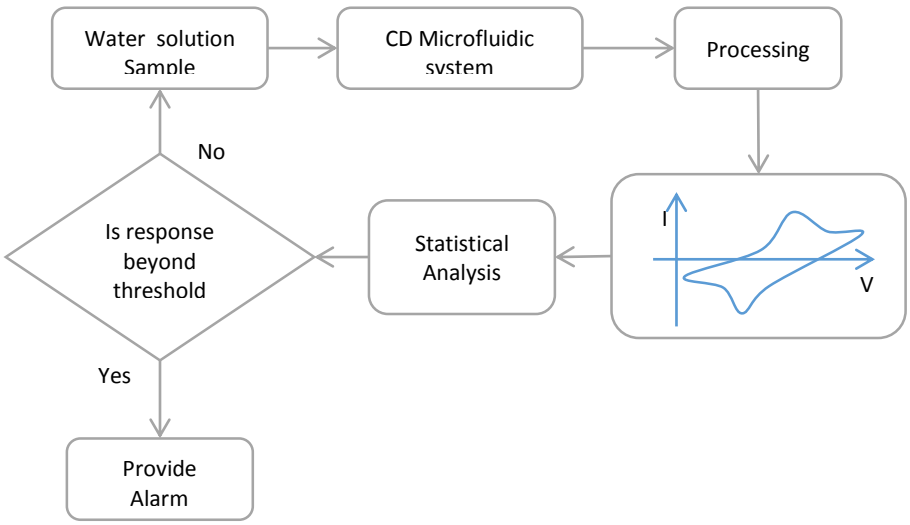

Figure 5.1 Flow diagram of response system using a CD platform and custom monitoring device

A more detailed explanation of the CD system and their characteristics are presented on appendix A. The appendix A covers operation theory of the CD, construction of Spin station for CD's and test of heating and cooling samples inside a CD.

Appendix A: CD Microfluidics

Sample preparation is an important step before solution measurement. Desired optimal conditions are expected during preparation to assure the results during measurement are closest to expected ideal response. Also during measurement these ideal conditions must be preserved trough the duration of the experiment. To maintain these conditions samples and methodologies must follow a precise experimental design so results are expected to theoretical data, achieving a minimum waste of resources. CD microfluidics are a platform where experimental parameters and near ideal conditions can be maintained for the duration of the experiment with controlled quantities of samples.

A.1 State of the Art and Principles of operation

Microstructures etched inside a CD represent an alternative model for the parallel preparation and analysis of samples in a controlled environment with advantage of combine these on the same disc. Another advantage of CD systems are the use of only centrifugal forces and capillary effects to control flow inside reservoirs and chambers in the CD without the use of valves. Even though centrifugal and capillary are the most common forces during analyses, they are complemented in most cases by external forces that complement the experiment, like heat radiation, contact cooling and heating and magnetic forces to increase the number of applications in a CD. Some of the applications for CD microfluidics are the separation of blood plasma [88], dielectrophoresis [89], multiplexed immunoassays [90] and PCR amplification [91].

Typically, a microfluidic CD contains a reservoir chamber where a sample is stored or prepared beforehand and sealed inside, this chamber can connect to a reaction chamber for measuring with a given process depending of the material and sample contained and at the end a waste site for disposal. Other chambers can be included with different functions like mixing, splitting, measuring, separation for a wider array of sample preparation and measurement.

To comprehend how the centrifugal force can move a liquid, an equation that relates the velocity of a CD and average velocity of a fluid (U) and volumetric flow (Q) are presented next [92]:

$$U = \frac{D_h^2 \rho \omega^2 \bar{r} \Delta r}{32 \mu L} \tag{6.1}$$

$$Q = UA \tag{6.2}$$

From equation 6.1 and 6.2, *Dh* is the hydraulic diameter of the channel (also defined as *4A/P* where *A* is the cross-sectional area and *P* is the wetted perimeter of the channel), ρ is the density of the liquid, ω is the angular velocity of the CD, $\bar{r}$ is the average distance of the liquid in the channel to the center of the disk, Δr is the radial extent of the fluid, μ is the viscosity of the solution, and *L* is the length of the liquid in the capillary channel. Figure A1.1 presents a microfluidic CD with some of these indicated parameters.

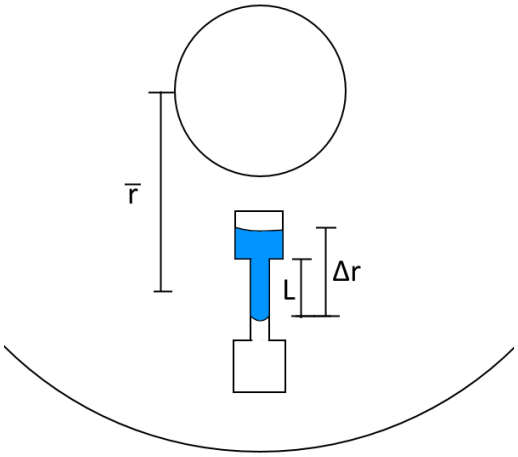

Figure A.1: Representation of a Microfluidic CD with internal chambers. The liquid inside the chambers is moved with rotary energy and capillary effects

To control the fluid in the CD, two types of valves are used, hydrophobic valves which decrease abruptly the hydrophobic cross-section channel and capillary valves that stop the liquid with a capillary pressure barrier at junction where the channel diameter suddenly expands. For the liquid to overcome the sudden narrowing of the hydrophobic valve, require a pressure Δp calculated as:

$$\Delta p = 2\sigma_L \cos(\theta_c)\left[\left(\frac{1}{w_1}\right) + \left(\frac{1}{h_1}\right)\right] - \left[\left(\frac{1}{w_2}\right) + \left(\frac{1}{h_2}\right)\right] \tag{6.3}$$

Where σ_L is the liquid surface tension, θ_c is the contact angle, w_1 and h_1 are the width and height of the channel before restriction and w_2 and h_2 width and height of the channel after restriction. With capillary valves, to allow the flow of liquid, the liquid pressure at the meniscus (P_m) from the centripetal force must be less or equal to the capillary barrier pressure (P_{cb}). The equations describing this forces are presented next:

$$P_{cb} = \frac{4\gamma_{al}\sin\theta_c}{D_h} \tag{6.4}$$

$$P_m = \rho\omega^2\bar{r}\Delta r \tag{6.5}$$

Where γ_{al} is the surface energy per unit area of the liquid-air is interface and θ_c is the contact angle.

A.2 Design and Analysis of rotating platform for CD Applications

Development of CD microfluidics present challenge not only in the design of the disc itself, but also the rotary platform that is needed in order to implement a CD system.

A rotary platform must provide support for a CD to achieve the required control of revolutions per minute (rpm) for the custom CD application, have a clear view of the CD for microscope monitoring or fluorescent measurements, depending of the application, systems

to heat, cool and connect electrically the spinning disc and protection for the user. A rotary platform for CD was designed and constructed at University of California, Irvine (UCI) for handling and testing microfluidics CDs in PCR applications, figure A1.2 shows the rotatory platform design and figure A1.3 the finished design.

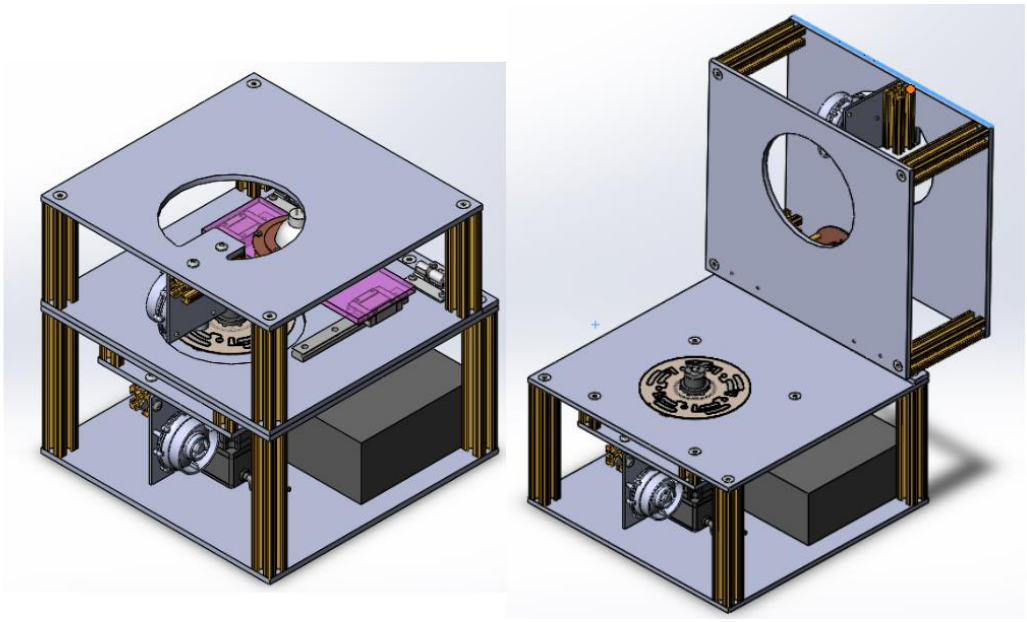

Figure A.2: Solidworks design of rotatory platform. This platform can move the CD at specific rpm and heat specific sections of the CD

With the design ready, fabrication of the platform using aluminum extrudes, plates, and external components, a safe rotary platform was build.

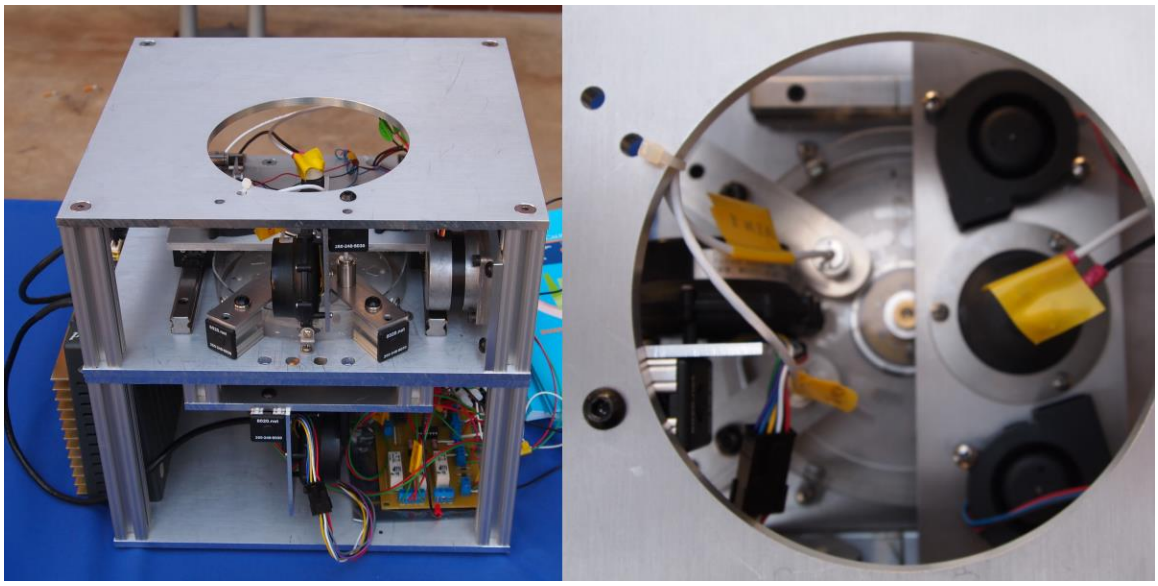

Figure A.3: Finished rotary platform, Front view (left), top view and opening for microscope (right)

The current rotating platform contains a slip ring mounted over a brushless motor for electrical contact to the disc which are used for electrodes inside a CD [89], [93] or connections to external components to the disc as thermistors or resistors. Blowers are installed on top and the bottom of the microfluidic CD holder for quick removing of heat form other techniques that use a high temperature for a process or experiment that also requires a quick cooling. The slip ring is mounted over a brushless motor connected to a motor controller, this allows to control the rpm, acceleration and general movement of the CD using a computer connected through a serial port. Over the CD is mounted an IR lamp on a moving rail pulled by a step motor and cooled by two mini blowers, the purpose of this lamp is to heat a specific band on the CD by moving the rail to a specific position and concentrate light in a specific radius The specific heat on only one part of the CD is needed for pneumatic methodologies [94], [95] and other process that need heat in specific zones [91], [96]. IR sensors are mounted at different radius for measuring of temperature on the CD surface.

For the control of these components and logging of information, a printed circuit board (PCB) connected to a computer is paced between the power connections of sensors, blowers, lamp and electric contacts on the slip ring and control is gained by activation or deactivating relays acting as on-off switches and voltage control pro the IR lamp.

A.3 Heat Transfer on CD

For validation on heating and cooling samples inside microfluidic CDs several test on different discs and combinations of blowers, heat resistors and IR lamp where used for the characterization of heating and cooling profiles. For heating, three heat sources are used, heat resistors (10Ω, 25W) that are solder to circular pcb and activated by the contacts on the slip ring, and IR lamp (12V 100W) controlled with voltage from the control pcb and a peltier element to heat with a controlled voltage. Cooling is done with blowers at the bottom and top of the CD using air at room temperature (25ºC). Different kinds of CDs are also introduced, the principal differences are the polycarbonate bottom of the disc which it may be transparent or black as seen on figure A.4.

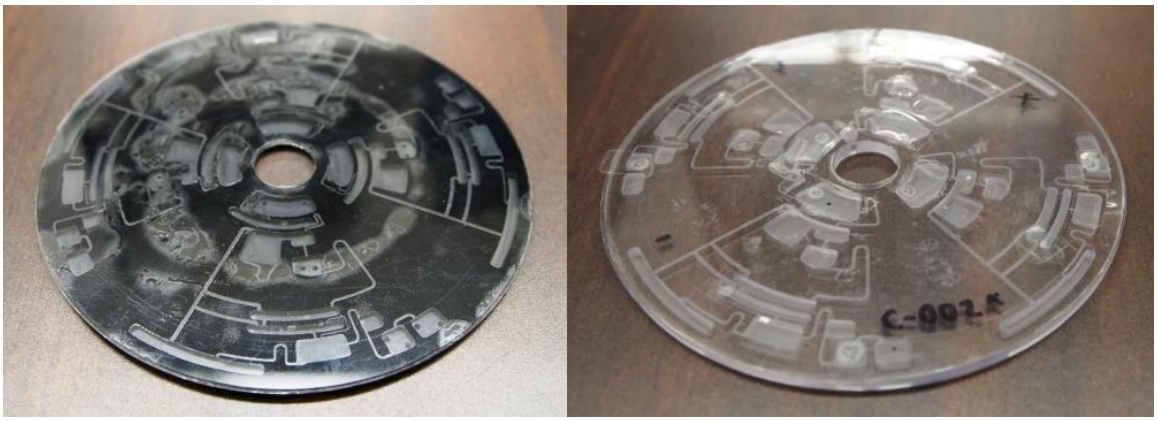

Figure A.4: Microfluidic CD made for different polycarbonate sheets. Black CD (left) and Transparent CD (right)

Measurements of temperatures on the sample are made with two methods; the first is using two IR sensors on top of the disc which produce a voltage that varies lineally with the temperature at a slope of 10mV/ºC. The second measurement uses a thermistor that is introduced inside the chamber (figure A.5) with the sample to heat and cool, this element changes in resistance depending of the temperature according to a logarithmic scale. With this information, we can create plots of temperature versus time on top and inside the sample for a very precise measurement of temperature.

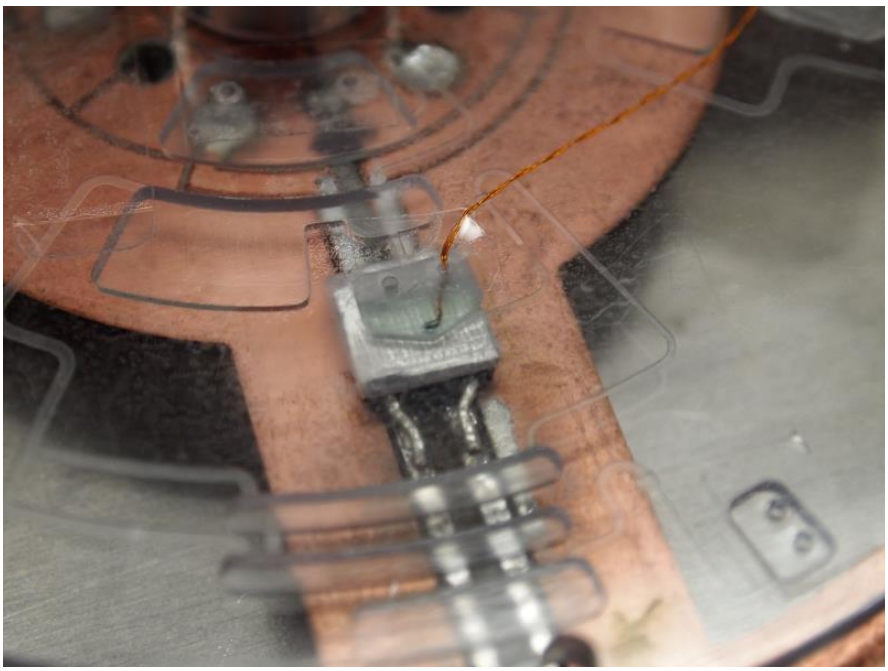

Figure A.5: Microfluidic chamber with water as biological sample and thermistor for temperature measuring

The first tests are done using a back disc, during the experiments a setpoint of 95°C is marked on the control system so the temperature is increased form room temperature to this value using the IR lamp or resistor. After reaching 95°C, the setpoint is moved to 30°C and blowers activated for cooling.

The results from these experiments are presented in the figure A.6 plots that compare heating and cooling curves using IR lamp, resistors and blowers; table A.1 presents heating and cooling rates obtained from the slopes of the curves from figure A.6:

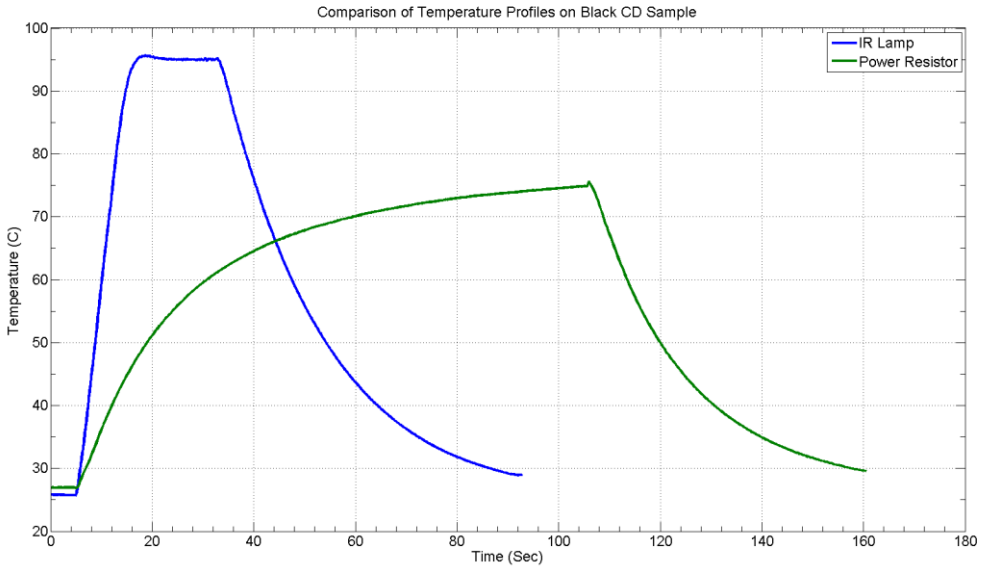

Figure A.6: Comparison of temperature profiles on black disc using IR lamp (blue line) and power resistor (green line)

Table 6.1 Calculated heating and cooling rates form figure A.6 lines from black disc measurements

	Sample Measurement		Surface Measurement	
Heat Source	Heating Rate (°C/s)	Cooling Rate (°C/s)	Heating Rate (°C/s)	Cooling Rate (°C/s)
IR Lamp	4.68	-0.87	6.90	-1.12
Resistor	0.46	-0.87	0.038	-0.06

From results obtained and presented on figure A.6 and table A.1, the black disc presents better heating and cooling rates using the IR lamp. Resistor heating presents a very slow rate of heating but due to the low temperatures over the disc, it may be more practical for handling in specific situations.

Tests over the transparent disc are divided on two categories depending on whether the sample chamber is routed under to allow the heat resistor closer to the sample (figure A.7). On the routed disc, an aluminum foil placed under the chamber between the resistor and the disc to increase the heat transfer between sample and resistor and to seal the open chamber.

Figure A.7: Difference between disc without routing on the bottom (left) and routed (right)

Results for heat transfer on transparent disc are presented in figures A.8 and A.9 with a comparison between disc heat and cooling rates on table A.2

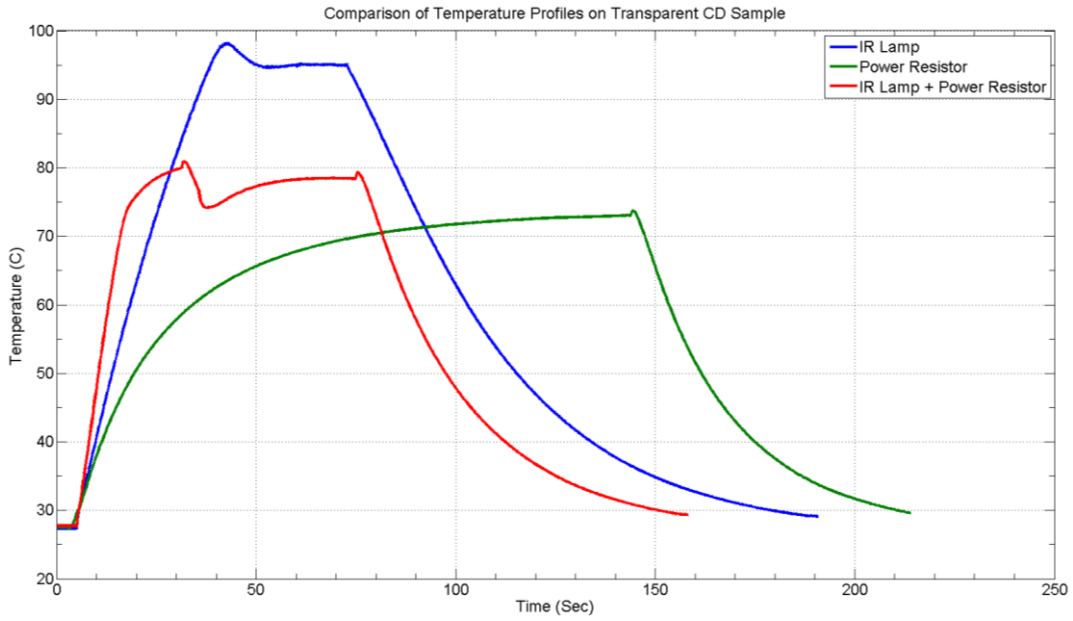

Figure A.8: Comparison of temperature profiles of transparent disc samples using IR lamp, resistor and IR lamp + resistor

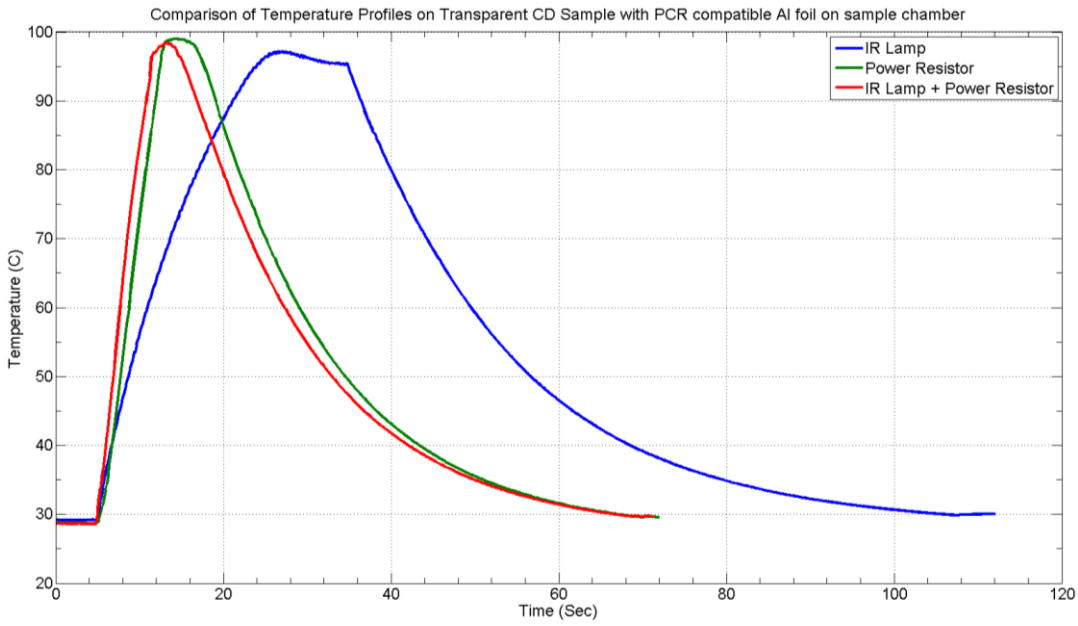

Figure A.9: Comparison of temperature profiles on transparent disc samples with aluminum foil using IR lamp, resistor and IR lamp + resistor

Table A.2: Comparison of heating and cooling rates on transparent disc calculated from the slopes in figures A.8 and A.9

	Sample Measurement		Surface Measurement	
Heat Source	Heating Rate (°C/s)	Cooling Rate (°C/s)	Heating Rate (°C/s)	Cooling Rate (°C/s)
IR	2.01	-0.61	2.34	-0.69
Resistor	0.33	-0.66	0.024	-0.03
IR + Resistor	3.85	-0.67	3.45	-0.15
IR (Al foil)	3.48	-0.92	3.32	-0.97
Resistor (Al foil)	8.82	-1.35	0.01	-0.05
IR + Resistor (Al foil)	10.30	-1.30	2.30	-0.25

Results in table A.2 reveal an increase in temperature rates when using the combined IR lamp and resistor, but is improved almost three times when combined with the aluminum foil under the chamber. Comparing results form table A.1 and A.2 we see that heat transfer is high in IR light on the black disc due to the absorption of more energy thanks to the black color.

6.4 Summary

Handling of small samples and preparation of these are an important part of the experimentation process, without it, results are not reliable enough and may not be reproducible. CD microfluidics offers a solution to the sample preparation, measurement and disposal concentrating all these steps in an inexpensive unique disc system. Centrifugal and capillary forces move the reagents and samples in the disc to the chambers where preparation

or measurement is done. Also external forces like heat, light or cooling are implemented to the disc to increase the treatments to the sample in the disc. For implementation of a CD system, a custom rotary platform with a variable speed, control of external forces, and microscope is used. Control of this platform is done with a PC and Labview software which collects measurements of temperature, rpm of the disc and data form the sample.

The principal focus on CD research for this work is the heat transmission to a sample inside a CD from an IR lamp and a power resistor. The characteristics of the IR lamp allow the transmission of heat through radiation while the power resistor transmits this energy through contact. Test on two different discs (black and transparent) demonstrate how the heat transmits differently between them. For the black disc test with only IR lamp and resistor demonstrate the heating rate is 10 times faster with IR light than with the resistors. For tests with the transparent disc, two different disc are implemented, one with the bottom layer intact and another with a small opening under the chamber with aluminum foil as a base. Heating rates with IR lamp are lower on the disc with Al foil, with a small increase on the disc without it but still lower compared to the black disc. Heat rate on the resistor was increased over three times compared to the IR heating on the disc with Al foil, surpassing those of the black CD. These results demonstrate forms in which the CD technology can be improved for a better heat transmission for several kinds of reactions depending of the heat transfer rates.

Bibliography

[1] T. Lindell and E. Welch, *Ecological Effects of Waste Water*. Routledge, 1992.

[2] R. Sykes and H. Walker, *The Civil Engineering Handbook, Second Edition*, vol. 20021369. CRC Press, 2002.

[3] D. Chapman, Ed., *Water Quality Assessments*. Taylor & Francis, 1996.

[4] M. Rudenko, *Handbook of Optofluidics*. CRC Press, 2010, p. A–1–A–5.

[5] R. Helmer and I. Hespanhol, *Water Pollution Control*. Taylor & Francis, 1998.

[6] M. La Farré, S. Pérez, L. Kantiani, and D. Barceló, "Fate and toxicity of emerging pollutants, their metabolites and transformation products in the aquatic environment," *TrAC Trends Anal. Chem.*, vol. 27, no. 11, pp. 991–1007, Dec. 2008.

[7] R. Rosal, M. S. Gonzalo, K. Boltes, P. Letón, J. J. Vaquero, and E. García-Calvo, "Identification of intermediates and assessment of ecotoxicity in the oxidation products generated during the ozonation of clofibric acid.," *J. Hazard. Mater.*, vol. 172, no. 2–3, pp. 1061–8, Dec. 2009.

[8] Organization World Health and International Programme on Chemical Safety, "Phenol / published under the joint sponsorship of the United Nations Environment Programme, the International Labour Organisation, and the World Health Organization," *Geneva : World Health Organization*, 1994. [Online]. Available: http://www.who.int/iris/handle/10665/39825.

[9] D. D. Snow, S. L. Bartelt-Hunt, S. E. Saunders, and D. a. Cassada, "Detection, Occurrence, and Fate of Emerging Contaminants in Agricultural Environments," *Water Environ. Res.*, vol. 79, no. 10, pp. 1061–1084, Oct. 2007.

[10] D. Pozar, "Microwave Network Analysis," in *Microwave Engineering*, 3rd ed., New York: Wiley, 2005, pp. 162–216.

[11] Y. Wang, Q. He, Y. Dong, and H. Chen, "In-channel modification of biosensor electrodes integrated on a polycarbonate microfluidic chip for micro flow-injection amperometric determination of glucose," *Sensors Actuators B Chem.*, vol. 145, no. 1, pp. 553–560, Mar. 2010.

[12] P. Patel and G. H. Markx, "Dielectric measurement of cell death," *Enzyme Microb. Technol.*, vol. 43, no. 7, pp. 463–470, Dec. 2008.

[13] P. M. Patel, A. Bhat, and G. H. Markx, "A comparative study of cell death using electrical capacitance measurements and dielectrophoresis," *Enzyme Microb. Technol.*, vol. 43, no. 7, pp. 523–530, Dec. 2008.

[14] M. Marzinotto, C. Santulli, and C. Mazzetti, "Dielectric properties of oil palm-natural rubber biocomposites," *2007 Annu. Rep. - Conf. Electr. Insul. Dielectr. Phenom.*, no. 1, pp. 584–587, 2007.

[15] M. Thein, F. Asphahani, A. Cheng, R. Buckmaster, M. Zhang, and J. Xu, "Response characteristics of single-cell impedance sensors employed with surface-modified microelectrodes.," *Biosens. Bioelectron.*, vol. 25, no. 8, pp. 1963–9, Apr. 2010.

[16] L. Jianhui, W. Xiaoming, H. Pengsheng, R. Tianling, and L. Litian, "Impedance spectroscopy analysis of cell-electrode interface.," *Conf. Proc. IEEE Eng. Med. Biol. Soc.*, vol. 7, pp. 7608–11, Jan. 2005.

[17] Z. Xi, Z. Stoynov, D. Vladikova, and N. Nuncho, "Capacitive Impedance Spectroscopy measuring system," in *2009 IEEE 9th International Conference on the Properties and Applications of Dielectric Materials*, 2009, pp. 1092–1093.

[18] S. Mohanty, S. Ravula, K. L. Engisch, and A. B. Frazier, "A micro system using dielectrophoresis and electrical impedance spectroscopy for cell manipulation and analysis," in *TRANSDUCERS '03. 12th International Conference on Solid-State Sensors, Actuators and Microsystems. Digest of Technical Papers (Cat. No.03TH8664)*, 2003, vol. 2, pp. 1055–1058.

[19] Y.-S. Liu, P. P. Banada, S. Bhattacharya, A. K. Bhunia, and R. Bashir, "Electrical characterization of DNA molecules in solution using impedance measurements," *Appl. Phys. Lett.*, vol. 92, no. 14, p. 143902, 2008.

[20] S. Zheng, M. S. Nandra, C.-Y. Shih, W. Li, and Y.-C. Tai, "Resonance impedance sensing of human blood cells," *Sensors Actuators A Phys.*, vol. 145–146, pp. 29–36, Jul. 2008.

[21] S. O. Nelson, "Agricultural applications of dielectric measurements," *IEEE Trans. Dielectr. Electr. Insul.*, vol. 13, no. 4, pp. 688–702, Aug. 2006.

[22] K. Fukunaga, S. Watanabe, and Y. Yamanaka, "Dielectric Properties of Tissue-Equivalent Liquids and Their Effects on Specific Absorption Rate," *IEEE Trans. Electromagn. Compat.*, vol. 46, no. 1, pp. 126–129, Feb. 2004.

[23] M. H. Moussa, M. A. Abu-Khousa, and N. N. Qaddoumi, "Measurement of liquids dielectric property using monopole probes operating at microwave frequencies," in *10th IEEE International Conference on Electronics, Circuits and Systems, 2003. ICECS 2003. Proceedings of the 2003*, 2003, pp. 1204–1207.

[24] S. Trabelsi and S. O. Nelson, "Nondestructive Sensing of Physical Properties of Granular Materials by Microwave Permittivity Measurement," *IEEE Trans. Instrum. Meas.*, vol. 55, no. 3, pp. 953–963, Jun. 2006.

[25] J. Sheen, “Microwave Dielectric Properties Measurements Using the Waveguide Reflection Dielectric Resonator,” in *2007 IEEE Instrumentation & Measurement Technology Conference IMTC 2007*, 2007, vol. 2, no. c, pp. 1–4.

[26] M. Kostopoulou and A. Nikolaou, “Analytical problems and the need for sample preparation in the determination of pharmaceuticals and their metabolites in aqueous environmental matrices,” *TrAC Trends Anal. Chem.*, vol. 27, no. 11, pp. 1023–1035, Dec. 2008.

[27] C.-J. Chung, P.-T. Hsieh, J.-F. Lin, C.-L. Wei, W.-T. Chang, C.-T. Chen, Y.-C. Chen, C.-C. Cheng, C.-H. Lin, K.-C. Chiu, S.-J. Chen, and K.-S. Kao, “Investigation of acoustic properties and Raman scattering of AlN films for biosensor application,” *2011 6th IEEE Int. Conf. Nano/Micro Eng. Mol. Syst.*, pp. 618–621, Feb. 2011.

[28] D. Li, D.-W. Li, J. S. Fossey, and Y.-T. Long, “Portable surface-enhanced Raman scattering sensor for rapid detection of aniline and phenol derivatives by on-site electrostatic preconcentration.,” *Anal. Chem.*, vol. 82, no. 22, pp. 9299–305, Nov. 2010.

[29] “Evaluation of analytical instrumentation. Part XXII Instrumentation for liquid chromatography/mass spectrometry,” *Accredit. Qual. Assur.*, vol. 12, no. 1, pp. 3–11, Oct. 2006.

[30] K. Grudpan, S. Lapanantnoppakhun, S. K. Hartwell, K. Watla-iad, W. Wongwilai, W. Siriangkhawut, W. Jangbai, W. Kumutanat, P. Nuntaboon, and S. Tontrong, “Simple lab-on-chip approach with time-based detection.,” *Talanta*, vol. 79, no. 4, pp. 990–4, Sep. 2009.

[31] C. E. Banks, T. J. Davies, G. G. Wildgoose, and R. G. Compton, “Electrocatalysis at graphite and carbon nanotube modified electrodes: edge-plane sites and tube ends are the reactive sites.,” *Chem. Commun. (Camb).*, no. 7, pp. 829–41, Feb. 2005.

[32] L. Ji and X. Zhang, “Fabrication of porous carbon nanofibers and their application as anode materials for rechargeable lithium-ion batteries.,” *Nanotechnology*, vol. 20, no. 15, p. 155705, Apr. 2009.

[33] R. R. Moore, C. E. Banks, and R. G. Compton, “Basal plane pyrolytic graphite modified electrodes: comparison of carbon nanotubes and graphite powder as electrocatalysts.,” *Anal. Chem.*, vol. 76, no. 10, pp. 2677–82, May 2004.

[34] T. Deblonde, C. Cossu-Leguille, and P. Hartemann, “Emerging pollutants in wastewater: a review of the literature.,” *Int. J. Hyg. Environ. Health*, vol. 214, no. 6, pp. 442–8, Nov. 2011.

[35] N. Arnich, M.-C. Canivenc-Lavier, M. Kolf-Clauw, H. Coffigny, J.-P. Cravedi, K. Grob, A.-C. Macherey, D. Masset, R. Maximilien, J.-F. Narbonne, F. Nesslany, J.

Stadler, and J. Tulliez, “Conclusions of the French Food Safety Agency on the toxicity of bisphenol A.,” *Int. J. Hyg. Environ. Health*, vol. 214, no. 3, pp. 271–5, Jun. 2011.

[36] M. Bondesson, J. Jönsson, I. Pongratz, N. Olea, J.-P. Cravedi, D. Zalko, H. Håkansson, K. Halldin, D. Di Lorenzo, C. Behl, D. Manthey, P. Balaguer, B. Demeneix, J. B. Fini, V. Laudet, and J.-A. Gustafsson, “A CASCADE of effects of bisphenol A.,” *Reprod. Toxicol.*, vol. 28, no. 4, pp. 563–7, Dec. 2009.

[37] C. Erler and J. Novak, “Bisphenol a exposure: human risk and health policy.,” *J. Pediatr. Nurs.*, vol. 25, no. 5, pp. 400–7, Oct. 2010.

[38] N. Khalil, J. R. Ebert, L. Wang, S. Belcher, M. Lee, S. a Czerwinski, and K. Kannan, “Bisphenol A and cardiometabolic risk factors in obese children.,” *Sci. Total Environ.*, vol. 470–471, pp. 726–32, Feb. 2014.

[39] M. Kundakovic and F. a Champagne, “Epigenetic perspective on the developmental effects of bisphenol A.,” *Brain. Behav. Immun.*, vol. 25, no. 6, pp. 1084–93, Aug. 2011.

[40] J. R. Rochester, “Bisphenol A and human health: a review of the literature.,” *Reprod. Toxicol.*, vol. 42, pp. 132–55, Dec. 2013.

[41] B. S. Rubin, “Bisphenol A: an endocrine disruptor with widespread exposure and multiple effects.,” *J. Steroid Biochem. Mol. Biol.*, vol. 127, no. 1–2, pp. 27–34, Oct. 2011.

[42] P.-W. Hsieh, S. a Al-Suwayeh, C.-L. Fang, C.-F. Lin, C.-C. Chen, and J.-Y. Fang, “The co-drug of conjugated hydroquinone and azelaic acid to enhance topical skin targeting and decrease penetration through the skin.,” *Eur. J. Pharm. Biopharm.*, vol. 81, no. 2, pp. 369–78, Jun. 2012.

[43] R. a Corley, J. C. English, T. S. Hill, L. a Fiorica, and D. a Morgott, “Development of a physiologically based pharmacokinetic model for hydroquinone.,” *Toxicol. Appl. Pharmacol.*, vol. 165, no. 2, pp. 163–74, Jun. 2000.

[44] J. C. English and P. J. Deisinger, “Metabolism and disposition of hydroquinone in Fischer 344 rats after oral or dermal administration.,” *Food Chem. Toxicol.*, vol. 43, no. 3, pp. 483–93, Mar. 2005.

[45] Z.-M. Hu, Q. Zhou, T.-C. Lei, S.-F. Ding, and S.-Z. Xu, “Effects of hydroquinone and its glucoside derivatives on melanogenesis and antioxidation: Biosafety as skin whitening agents.,” *J. Dermatol. Sci.*, vol. 55, no. 3, pp. 179–84, Sep. 2009.

[46] C.-F. Hung, W.-Y. Chen, I. a Aljuffali, H.-C. Shih, and J.-Y. Fang, “The risk of hydroquinone and sunscreen over-absorption via photodamaged skin is not greater in

senescent skin as compared to young skin: nude mouse as an animal model.," *Int. J. Pharm.*, vol. 471, no. 1–2, pp. 135–45, Aug. 2014.

[47] P. J. Kerzic, W. S. Liu, M. T. Pan, H. Fu, Y. Zhou, a R. Schnatter, and R. D. Irons, "Analysis of hydroquinone and catechol in peripheral blood of benzene-exposed workers.," *Chem. Biol. Interact.*, vol. 184, no. 1–2, pp. 182–8, Mar. 2010.

[48] T. S. Poet, B. D. Carlton, J. a Deyo, and P. M. Hinderliter, "Hydroquinone PBPK model refinement and application to dermal exposure.," *Food Chem. Toxicol.*, vol. 48, no. 11, pp. 3085–92, Nov. 2010.

[49] D. C. Topping, L. G. Bernard, J. L. O'Donoghue, and J. C. English, "Hydroquinone: acute and subchronic toxicity studies with emphasis on neurobehavioral and nephrotoxic effects.," *Food Chem. Toxicol.*, vol. 45, no. 1, pp. 70–8, Jan. 2007.

[50] M. De Falco, A. Sellitti, R. Sciarrillo, A. Capaldo, S. Valiante, G. Iachetta, M. Forte, and V. Laforgia, "Nonylphenol effects on the HPA axis of the bioindicator vertebrate, Podarcis sicula lizard.," *Chemosphere*, vol. 104, pp. 190–6, Jun. 2014.

[51] S. Omeroğlu and F. D. Sanin, "Fate and degradation kinetics of nonylphenol compounds in aerobic batch digesters.," *Water Res.*, vol. 64C, pp. 1–12, Jul. 2014.

[52] B. Roig, A. Cadiere, S. Bressieux, S. Biau, S. Faure, and P. de Santa Barbara, "Environmental concentration of nonylphenol alters the development of urogenital and visceral organs in avian model.," *Environ. Int.*, vol. 62, pp. 78–85, Jan. 2014.

[53] P. Gao, Z. Li, M. Gibson, and H. Gao, "Ecological risk assessment of nonylphenol in coastal waters of China based on species sensitivity distribution model.," *Chemosphere*, vol. 104, pp. 113–9, Jun. 2014.

[54] X. Liao, C. Zhang, L. Yao, J. Li, M. Liu, L. Xu, and M. Evalde, "Sorption behavior of nonylphenol (NP) on sewage-irrigated soil: kinetic and thermodynamic studies.," *Sci. Total Environ.*, vol. 473–474, pp. 530–6, Mar. 2014.

[55] a Soares, B. Guieysse, B. Jefferson, E. Cartmell, and J. N. Lester, "Nonylphenol in the environment: a critical review on occurrence, fate, toxicity and treatment in wastewaters.," *Environ. Int.*, vol. 34, no. 7, pp. 1033–49, Oct. 2008.

[56] J. Hwang, S.-S. Suh, M. Chang, S. Yun Park, T. K. Ryu, S. Lee, and T.-K. Lee, "Effects of triclosan on reproductive prarmeters and embryonic development of sea urchin, Strongylocentrotus nudus.," *Ecotoxicol. Environ. Saf.*, vol. 100, pp. 148–52, Feb. 2014.

[57] S. Villa, M. Vighi, and A. Finizio, "Experimental and predicted acute toxicity of antibacterial compounds and their mixtures using the luminescent bacterium Vibrio fischeri.," *Chemosphere*, vol. 108, pp. 239–44, Aug. 2014.

[58] X. Wang, Z. Liu, W. Wang, Z. Yan, C. Zhang, W. Wang, and L. Chen, “Assessment of toxic effects of triclosan on the terrestrial snail (Achatina fulica).,” *Chemosphere*, vol. 108, pp. 225–30, Aug. 2014.

[59] V. Matozzo, N. Franchi, and L. Ballarin, “In vitro effects of the nonsteroidal anti-inflammatory drug, ibuprofen, on the immune parameters of the colonial ascidian Botryllus schlosseri.,” *Toxicol. In Vitro*, vol. 28, no. 5, pp. 778–83, Aug. 2014.

[60] I. Moro, V. Matozzo, A. Piovan, E. Moschin, and F. D. Vecchia, “Morpho-physiological effects of Ibuprofen by Scenedesmus rubescens,” *Environ. Toxicol. Pharmacol.*, Jul. 2014.

[61] M. Parolini, A. Binelli, and A. Provini, “Chronic effects induced by ibuprofen on the freshwater bivalve Dreissena polymorpha.,” *Ecotoxicol. Environ. Saf.*, vol. 74, no. 6, pp. 1586–94, Sep. 2011.

[62] M. Saravanan, K. U. Devi, a Malarvizhi, and M. Ramesh, “Effects of Ibuprofen on hematological, biochemical and enzymological parameters of blood in an Indian major carp, Cirrhinus mrigala.,” *Environ. Toxicol. Pharmacol.*, vol. 34, no. 1, pp. 14–22, Jul. 2012.

[63] J. Aldekoa, C. Medici, V. Osorio, S. Pérez, R. Marcé, D. Barceló, and F. Francés, “Modelling the emerging pollutant diclofenac with the GREAT-ER model: application to the Llobregat River Basin.,” *J. Hazard. Mater.*, vol. 263 Pt 1, pp. 207–13, Dec. 2013.

[64] U. Boelsterli, “Diclofenac-induced liver injury: a paradigm of idiosyncratic drug toxicity,” *Toxicol. Appl. Pharmacol.*, vol. 192, no. 3, pp. 307–322, Nov. 2003.

[65] J.-P. Chae, M. S. Park, Y.-S. Hwang, B.-H. Min, S.-H. Kim, H.-S. Lee, and M.-J. Park, “Evaluation of developmental toxicity and teratogenicity of diclofenac using Xenopus embryos.,” *Chemosphere*, vol. 120C, pp. 52–58, Jun. 2014.

[66] D. M. Odom, D. M. Mladsi, K. G. Saag, B. N. Sherif, L. Miles, N. Ronquest, and J. Wang, “Relationship between diclofenac dose and risk of gastrointestinal and cardiovascular events: meta-regression based on two systematic literature reviews.,” *Clin. Ther.*, vol. 36, no. 6, pp. 906–17, Jun. 2014.

[67] M. Persson, A. F. Løye, T. Mow, and J. J. Hornberg, “A high content screening assay to predict human drug-induced liver injury during drug discovery.,” *J. Pharmacol. Toxicol. Methods*, vol. 68, no. 3, pp. 302–13, 2013.

[68] S. Ramm and A. Mally, “Role of drug-independent stress factors in liver injury associated with diclofenac intake.,” *Toxicology*, vol. 312, pp. 83–96, Oct. 2013.

[69] H. Yu, E. Nie, J. Xu, S. Yan, W. J. Cooper, and W. Song, “Degradation of diclofenac by advanced oxidation and reduction processes: kinetic studies, degradation pathways and toxicity assessments.,” *Water Res.*, vol. 47, no. 5, pp. 1909–18, Apr. 2013.

[70] K. Ghasemi, A. R. Rezvani, M. M. Rosli, I. Abdul Razak, A. Moghimi, and F. Ghasemi, “Potential antidiabetic drug involving a zinc anionic complex of dipic and metformin as counter ions: Synthesis, characterization, crystal structure and electrochemical studies,” *J. Mol. Struct.*, vol. 1074, pp. 79–84, Sep. 2014.

[71] E. Badrick and A. G. Renehan, “Diabetes and cancer: 5years into the recent controversy.,” *Eur. J. Cancer*, vol. 50, no. 12, pp. 2119–25, Aug. 2014.

[72] M. Barnea, T. Cohen-Yogev, N. Chapnik, Z. Madar, and O. Froy, “Effect of metformin and lipid emulsion on the circadian gene expression in muscle cells.,” *Int. J. Biochem. Cell Biol.*, vol. 53, pp. 151–61, Aug. 2014.

[73] R. Khang, C. Park, and J.-H. Shin, “The biguanide metformin alters phosphoproteomic profiling in mouse brain.,” *Neurosci. Lett.*, vol. 579C, pp. 145–150, Jul. 2014.

[74] C. Li and D. Kong, “Cancer risks from diabetes therapies: Evaluating the evidence.,” *Pharmacol. Ther.*, May 2014.

[75] Y. Liu, G. Tang, Z. Zhang, Y. Wang, and G.-Y. Yang, “Metformin promotes focal angiogenesis and neurogenesis in mice following middle cerebral artery occlusion.,” *Neurosci. Lett.*, vol. 579, pp. 46–51, Jul. 2014.

[76] D. Weckermann, “Re: Metformin use and all-cause and prostate cancer-specific mortality among men with diabetes.,” *Eur. Urol.*, vol. 66, no. 1, pp. 174–5, Jul. 2014.

[77] S. Aburuz, J. Millership, and J. McElnay, “The development and validation of liquid chromatography method for the simultaneous determination of metformin and glipizide, gliclazide, glibenclamide or glimperide in plasma.,” *J. Chromatogr. B. Analyt. Technol. Biomed. Life Sci.*, vol. 817, no. 2, pp. 277–86, Mar. 2005.

[78] K. F. Capes and R. Y. Wang, “CASE REPORT D elayed Hypoglycemia in a Child After Ingestion of a Single Glipizide Tablet,” no. June, pp. 3–6, 1998.

[79] E. M. Ghoneim, M. a El-Attar, E. Hammam, and P. Y. Khashaba, “Stripping voltammetric quantification of the anti-diabetic drug glipizide in bulk form and pharmaceutical formulation.,” *J. Pharm. Biomed. Anal.*, vol. 43, no. 4, pp. 1465–9, Mar. 2007.

[80] C.-H. Kim, S.-H. Park, Y.-B. Sim, S.-S. Kim, S.-J. Kim, S.-M. Lim, J.-S. Jung, and H.-W. Suh, "Effect of tolbutamide, glyburide and glipizide administered supraspinally on CA3 hippocampal neuronal cell death and hyperglycemia induced by kainic acid in mice.," *Brain Res.*, vol. 1564, pp. 33–40, May 2014.

[81] S. M. Wanjerkhede, R. S. Bapi, and V. D. Mytri, "Reinforcement learning and dopamine in the striatum: A modeling perspective," *Neurocomputing*, vol. 138, pp. 27–40, Aug. 2014.

[82] B. J. Weiland, M. M. Heitzeg, D. Zald, C. Cummiford, T. Love, R. a Zucker, and J.-K. Zubieta, "Relationship between impulsivity, prefrontal anticipatory activation, and striatal dopamine release during rewarded task performance.," *Psychiatry Res.*, vol. 223, no. 3, pp. 244–52, Sep. 2014.

[83] A. Podder, N. Jatana, and N. Latha, "Human Dopamine Receptors Interaction Network (DRIN): A systems biology perspective on topology, stability and functionality of the network.," *J. Theor. Biol.*, vol. 357, pp. 169–83, Sep. 2014.

[84] S. M. Perez, L. Chen, and D. J. Lodge, "Alterations in dopamine system function across the estrous cycle of the MAM rodent model of schizophrenia.," *Psychoneuroendocrinology*, vol. 47, pp. 88–97, Sep. 2014.

[85] L. Chandrakantha, "Learning ANOVA concepts using simulation," *... Eng. Educ. (ASEE Zo. 1), ...*, 2014.

[86] M. Diaconu, S. C. Litescu, and G. L. Radu, "Laccase–MWCNT–chitosan biosensor—A new tool for total polyphenolic content evaluation from in vitro cultivated plants," *Sensors Actuators B Chem.*, vol. 145, no. 2, pp. 800–806, Mar. 2010.

[87] R. S. Freire, N. Durán, and L. T. Kubota, "Effects of fungal laccase immobilization procedures for the development of a biosensor for phenol compounds.," *Talanta*, vol. 54, no. 4, pp. 681–6, May 2001.

[88] M. Amasia and M. Madou, "Large-volume centrifugal microfluidic device for blood plasma separation.," *Bioanalysis*, vol. 2, no. 10, pp. 1701–10, Oct. 2010.

[89] R. Martinez-Duarte, R. a Gorkin, K. Abi-Samra, and M. J. Madou, "The integration of 3D carbon-electrode dielectrophoresis on a CD-like centrifugal microfluidic platform.," *Lab Chip*, vol. 10, no. 8, pp. 1030–43, Apr. 2010.

[90] Z. Noroozi, H. Kido, R. Peytavi, R. Nakajima-Sasaki, A. Jasinskas, M. Micic, P. L. Felgner, and M. J. Madou, "A multiplexed immunoassay system based upon reciprocating centrifugal microfluidics.," *Rev. Sci. Instrum.*, vol. 82, no. 6, p. 064303, Jun. 2011.

[91] M. Amasia, M. Cozzens, and M. J. Madou, “Centrifugal microfluidic platform for rapid PCR amplification using integrated thermoelectric heating and ice-valving,” *Sensors Actuators B Chem.*, vol. 161, no. 1, pp. 1191–1197, Jan. 2012.

[92] J. V. Zoval and M. J. Madou, “Centrifuge-Based Fluidic Platforms,” *Proc. IEEE*, vol. 92, no. 1, pp. 140–153, Jan. 2004.

[93] Z. Noroozi, H. Kido, and M. J. Madou, “Electrolysis-Induced Pneumatic Pressure for Control of Liquids in a Centrifugal System,” *J. Electrochem. Soc.*, vol. 158, no. 11, p. P130, 2011.

[94] K. Abi-Samra, R. Hanson, M. Madou, and R. a Gorkin, “Infrared controlled waxes for liquid handling and storage on a CD-microfluidic platform.,” *Lab Chip*, vol. 11, no. 4, pp. 723–6, Feb. 2011.

[95] K. Abi-Samra, L. Clime, L. Kong, R. Gorkin, T.-H. Kim, Y.-K. Cho, and M. Madou, “Thermo-pneumatic pumping in centrifugal microfluidic platforms,” *Microfluid. Nanofluidics*, vol. 11, no. 5, pp. 643–652, Jun. 2011.

[96] J. Siegrist, R. Gorkin, M. Bastien, G. Stewart, R. Peytavi, H. Kido, M. Bergeron, and M. Madou, “Validation of a centrifugal microfluidic sample lysis and homogenization platform for nucleic acid extraction with clinical samples.,” *Lab Chip*, vol. 10, no. 3, pp. 363–71, Feb. 2010.